

Deriving an Accurate Formula of Scale-dependent Bias with Primordial Non-Gaussianity: An Application of the Integrated Perturbation Theory

Takahiko Matsubara*

*Kobayashi-Maskawa Institute for the Origin of Particles and the Universe,
Nagoya University, Chikusa, Nagoya, 464-8602, Japan; and
Department of Physics, Nagoya University, Chikusa, Nagoya, 464-8602, Japan
(Dated: March 6, 2013)*

We apply the integrated perturbation theory [1] to evaluate the scale-dependent bias in the presence of primordial non-Gaussianity. The integrated perturbation theory is a general framework of nonlinear perturbation theory, in which a broad class of bias models can be incorporated into perturbative evaluations of biased power spectrum and higher-order polyspectra. Approximations such as the high-peak limit or the peak-background split are not necessary to derive the scale-dependent bias in this framework. Applying the halo approach, previously known formulas are re-derived as limiting cases of a general formula in this work, and it is implied that modifications should be made in general situations. Effects of redshift-space distortions are straightforwardly incorporated. It is found that the slope of the scale-dependent bias on large scales is determined only by the behavior of primordial bispectrum in the squeezed limit, and is not sensitive to bias models in general. It is the amplitude of scale-dependent bias that is sensitive to the bias models. The effects of redshift-space distortions turn out to be quite small for the monopole component of the power spectrum, while the quadrupole component is proportional to the monopole component on large scales, and thus also sensitive to the primordial non-Gaussianity.

PACS numbers: 98.80.-k, 98.65.-r, 98.80.Cq, 98.80.Es

I. INTRODUCTION

The primordial non-Gaussianity is a useful indicator in searching for the generation mechanism of density fluctuations in the universe. While the primordial non-Gaussianity is small in the simplest model of single-field slow-roll inflation, there are various other inflationary models which predict fairly large primordial non-Gaussianities (for review, see Refs. [2, 3]). Alternative models without inflation can also produce large non-Gaussianities (see, e.g., Ref. [4]). Accordingly, constraining or detecting the primordial non-Gaussianity has a substantial importance in studying very early stages of the universe.

The large-scale structure (LSS) of the universe has been one of the most important ways of constraining cosmological models in general. In recent years, it was found that the primordial non-Gaussianity produces the scale-dependent bias in the LSS [5–7]. Although the scale-dependent bias from the primordial non-Gaussianity mainly appears on very large scales, the form of the scale dependence does not receive general relativistic corrections even on scales larger than the Hubble radius [8].

The scale-dependent bias as a method to constrain the primordial non-Gaussianity has already been applied to observational data of galaxies and quasars [9–12]. The constraints derived from the scale-dependent bias are competitive with the measurements in the cosmic microwave background (CMB). A hint of a positive value of local-type non-Gaussianity parameter f_{NL} was indicated by analyses of the scale-dependent bias [12], which could have profound implications for mod-

els of the early universe. However, more detailed analyses with large galaxy surveys are necessary to derive conclusive results.

On the theoretical side, analytic expressions for the scale-dependent bias has been only approximately derived. So far, at least three kinds of derivation are known. One is based on the method of peak-background split [5, 9, 13–18], and the other is based on the statistics of high-threshold regions [6, 17, 19, 20]. It is also shown that the scale-dependent bias generally appears in phenomenological models of local bias [21, 22]. Because those theoretical derivations are approximate and not exact, they should have been compared with numerical simulations [23–27]. The scale-dependent bias is qualitatively confirmed by simulations, although the detailed amplitude of the analytic predictions needs to be modified [16, 23, 27].

The purpose of this paper is to provide more precise and more general analytic expressions for the scale-dependent bias in the presence of primordial non-Gaussianity. Evolutions of density fluctuations on sufficiently large scales are expected to be described by the nonlinear perturbation theory. However, a consistent inclusion of the general form of bias in the nonlinear perturbation theory had not been clear until recently.

The integrated perturbation theory (IPT) [1] is the formalism in which a broad class of biasing scheme can be consistently included on a general ground. The local Eulerian biasing scheme has been frequently adopted in attempts of incorporating the bias into the nonlinear perturbation theory. However, the local Eulerian bias is not consistent with the nonlinear dynamics in general [1, 28], because the nonlinear evolutions are nonlocal phenomena. In the formalism of IPT, generally nonlocal biasing either in Eulerian and Lagrangian spaces can be consistently included in the nonlinear perturbation theory. The effects of primordial non-Gaussianity and

*Electronic address: taka@kmi.nagoya-u.ac.jp

redshift-space distortions are naturally incorporated into the formalism.

Consequently, it is a straightforward application of iPT to making predictions of scale-dependent bias in the presence of primordial non-Gaussianity. In this paper, we first present the most general prediction of iPT for the scale-dependent bias, which can be applied to almost any type of primordial non-Gaussianity and to almost any model of bias, as long as we consider the regime where the perturbation theory applies. We then consider popular models of primordial non-Gaussianity, i.e., local-, equilateral-, folded-, and orthogonal-type non-Gaussianities. Asymptotic behaviors of scale-dependent bias on large scales, which have been derived in limited cases in the literature, are re-derived in general situations without resorting to specific forms of bias. When the halo model of bias is adopted, the previously known formulas of scale-dependent bias are re-derived by taking appropriate limits of our general formula. In course of derivation, nonlocality of bias turns out to be important. We also show that previous formulas derived from the peak-background split are only consistent with the Press-Schechter mass function. When the mass function deviates from the Press-Schechter form, our general formula predicts that those previous formulas of scale-dependent bias should be corrected.

The main purpose of this paper is to show how the iPT can be applied to making theoretical predictions of the scale-dependent bias, and to give lowest-order calculations with primordial bispectra, when the bias is given by a simple, nonlocal model of halo bias. With the iPT formalism, predicting the scale-dependent bias is straightforward once the bias model is given. Theoretical uncertainties in predicting the scale-dependent bias are reduced to those of the bias model. Accurate modeling of biasing is actively studied in recent years. Once we have an accurate model of galaxy bias which is generally nonlocal, the iPT immediately gives predictions of scale-dependent bias with least approximations.

This paper is organized as follows. In Sections II–IV, analytic derivations of scale-dependent bias in real space are presented in order. The general formula of the biased power spectrum in real space with primordial bispectrum is derived by the lowest-order iPT in Sec. II. Large-scale limits of the scale-dependent bias in concrete models of primordial non-Gaussianity are generally investigated in Sec. III without assuming the models of bias. In Sec. IV, we consider the shapes of renormalized bias functions which are needed in iPT. We generalize the previous results to include the effects of the smoothing function in the halo model of bias. Numerical evaluations of the analytic formula are presented and compared with previous predictions in Sec. V. In Sec. VI, we generalize our formula to include the redshift-space distortions. In Sec. VII, we summarize our results.

In plotting the figures of this paper, we adopt a cosmological model of flat curvature with parameters $\Omega_{m0} = 0.275$, $\Omega_{\Lambda0} = 1 - \Omega_{m0} = 0.725$, $\Omega_{b0} = \Omega_{m0} - \Omega_{c0} = 0.046$, $n_s = 0.96$, $\sigma_8 = 0.8$, $H_0 = 70 \text{ km/s/Mpc}$, where Ω_{m0} is the matter density parameter, $\Omega_{\Lambda0}$ is the cosmological constant parameter, Ω_{b0} is the baryon density parameter, Ω_{c0} is the cold dark matter density parameter, n_s and σ_8 are respectively the spectral

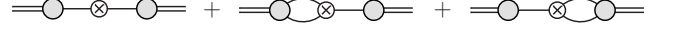


FIG. 1: The diagrammatic representation of the power spectrum in terms of multipoint propagators. Details of diagrammatic rules are described in Ref. [1].

index and the amplitude of primordial density fluctuations, and H_0 is the Hubble's constant.

II. INTEGRATED PERTURBATION THEORY AND SCALE-DEPENDENT BIAS FROM PRIMORDIAL NON-GAUSSIANITY

We apply the formalism of iPT to derive a general formula of the scale-dependent bias from the primordial non-Gaussianity, without assuming the peak-background split or the high-peak limit. In the derivation, it is convenient to introduce the multipoint propagators of biased objects. The multipoint propagators of mass and velocity fields are recently introduced in Ref. [29, 30], and those of biased objects are introduced in Ref. [1]. The multipoint propagators $\Gamma_X^{(n)}$ of biased objects X are defined by ensemble averages of functional derivatives

$$\left\langle \frac{\delta^n \delta_X(\mathbf{k})}{\delta \delta_L(\mathbf{k}_1) \cdots \delta \delta_L(\mathbf{k}_n)} \right\rangle = (2\pi)^{3-3n} \delta_D^3(\mathbf{k}_{1\dots n} - \mathbf{k}) \Gamma_X^{(n)}(\mathbf{k}_1, \dots, \mathbf{k}_n), \quad (1)$$

where $\delta_L(\mathbf{k})$ is the Fourier transform of the linear density field, and $\delta_X(\mathbf{k})$ is the Fourier transform of the number density field of the biased objects X in *Eulerian space*. On the right-hand side, $\mathbf{k}_{1\dots n} \equiv \mathbf{k}_1 + \cdots + \mathbf{k}_n$ and $\delta_D^3(\mathbf{k})$ is the Dirac's delta function in three dimensions.

In terms of the multipoint propagators, the biased power spectrum of objects X is represented by

$$P_X(k) = [\Gamma_X^{(1)}(\mathbf{k})]^2 P_L(k) + \Gamma_X^{(1)}(\mathbf{k}) \int \frac{d^3 k'}{(2\pi)^3} \Gamma_X^{(2)}(\mathbf{k}', \mathbf{k} - \mathbf{k}') B_L(k, k', |\mathbf{k} - \mathbf{k}'|) + \cdots, \quad (2)$$

where $P_L(k)$ is the linear power spectrum and $B_L(k_1, k_2, k_3)$ is the linear bispectrum. The diagrammatic representation of the above equation is shown in Fig. 1. The details of the diagrammatic rules are described in Ref. [1]. The multipoint propagators are represented by grey circles and the linear polyspectra are represented by crossed circles. The multipoint propagators include all the loop corrections at the corresponding vertices. For Gaussian initial conditions, the linear bispectrum is absent. In this paper, we consider only lowest-order contributions of the primordial non-Gaussianity which are linearly dependent on the bispectrum. Contributions from the trispectrum and higher-order polyspectra, and terms like a product of power spectrum and bispectrum are all neglected.

The multipoint propagators $\Gamma_X^{(1)}$ and $\Gamma_X^{(2)}$ also contain contributions from primordial non-Gaussianity in general. However, such contributions in Eq. (2) are higher orders in the

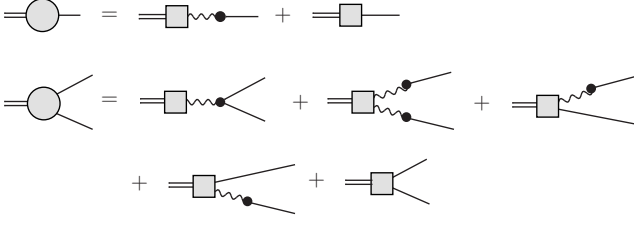


FIG. 2: Diagrammatic representations of the first two multipoint propagators with renormalized Lagrangian bias functions in the lowest-order approximation. Details of diagrammatic rules are described in Ref. [1].

above sense. Accordingly, we do not have to consider the non-Gaussian corrections to evaluate the multipoint propagators of Eq. (1) in the lowest-order approximation of this paper.

In the iPT, a concept of renormalizing Lagrangian bias functions is introduced. The renormalized bias functions in Lagrangian space c_n^L is defined by

$$c_n^L(\mathbf{k}_1, \dots, \mathbf{k}_n) = (2\pi)^{3n} \int \frac{d^3k}{(2\pi)^3} \left\langle \frac{\delta^n \delta_X^L(\mathbf{k})}{\delta \delta_L(\mathbf{k}_1) \dots \delta \delta_L(\mathbf{k}_n)} \right\rangle, \quad (3)$$

where $\delta_X^L(\mathbf{k})$ is the Fourier transform of the number density field of biased objects X in Lagrangian space. An equivalent way of defining the renormalized bias functions is given by

$$\left\langle \frac{\delta^n \delta_X^L(\mathbf{k})}{\delta \delta_L(\mathbf{k}_1) \dots \delta \delta_L(\mathbf{k}_n)} \right\rangle = (2\pi)^{3-3n} \delta_D^3(\mathbf{k}_{1\dots n} - \mathbf{k}) c_n^L(\mathbf{k}_1, \dots, \mathbf{k}_n). \quad (4)$$

In this form of definition, the similarity of the renormalized bias functions in Lagrangian space and the multipoint propagators of Eulerian space is obvious. The renormalized bias functions c_n^L can be seen as multipoint propagators of biasing in Lagrangian space. When the bias is not present, the number density field of objects is uniform in Lagrangian space, $\delta_X^L = 0$, and all the renormalized bias functions vanish.

Applying the diagrammatic methods of iPT [1] in the lowest-order approximation, the first and second multipoint propagators in terms of renormalized Lagrangian bias functions are given by

$$\Gamma_X^{(1)}(\mathbf{k}) = \mathbf{k} \cdot \mathbf{L}_1(\mathbf{k}) + c_1^L(k) \quad (5)$$

$$\begin{aligned} \Gamma_X^{(2)}(\mathbf{k}_1, \mathbf{k}_2) = & \mathbf{k} \cdot \mathbf{L}_2(\mathbf{k}_1, \mathbf{k}_2) + [\mathbf{k} \cdot \mathbf{L}_1(\mathbf{k}_1)][\mathbf{k} \cdot \mathbf{L}_1(\mathbf{k}_2)] \\ & + \mathbf{k} \cdot \mathbf{L}_1(\mathbf{k}_1) c_1^L(k_2) + \mathbf{k} \cdot \mathbf{L}_1(\mathbf{k}_2) c_1^L(k_1) \\ & + c_2^L(\mathbf{k}_1, \mathbf{k}_2), \end{aligned} \quad (6)$$

where \mathbf{L}_n is the n th order perturbation kernel of displacement field, and $\mathbf{k} = \mathbf{k}_1 + \mathbf{k}_2$ in Eq. (6). The diagrams for the above expressions are shown in Fig. 2. The correspondences between diagrams and equations are detailed in Ref. [1]. We omit partial resummations of the displacement field Ψ . If we leave these partial resummations, the right-hand sides of Eqs. (5) and (6) are multiplied by a factor $\Pi(\mathbf{k}) = \langle e^{-i\mathbf{k} \cdot \Psi} \rangle$. This factor is almost unity on sufficiently large scales. Moreover, this factor is cancelled when we calculate the scale-dependent bias $\Delta b(k)$ of Eq. (22) below. Therefore, we do

not include this factor from the first place. One should note that Eqs. (5) and (6) are lowest-order results. For higher-order calculations, loop corrections to the tree-level expressions of Eqs. (5) and (6) for multipoint propagators should be included as depicted in Fig. 17 of Ref. [1].

The perturbation kernels \mathbf{L}_n are calculated by the Lagrangian perturbation theory [31–37]. In real space, the first two kernels are given by

$$\mathbf{L}_1(\mathbf{k}) = \frac{\mathbf{k}}{k^2}, \quad (7)$$

$$\mathbf{L}_2(\mathbf{k}_1, \mathbf{k}_2) = \frac{3}{7} \frac{\mathbf{k}_{12}}{k_{12}^2} \left[1 - \left(\frac{\mathbf{k}_1 \cdot \mathbf{k}_2}{k_1 k_2} \right)^2 \right], \quad (8)$$

and Eqs. (5) and (6) reduce to

$$\Gamma_X^{(1)}(\mathbf{k}) = 1 + c_1^L(k) \quad (9)$$

$$\begin{aligned} \Gamma_X^{(2)}(\mathbf{k}_1, \mathbf{k}_2) = & F_2(\mathbf{k}_1, \mathbf{k}_2) + \left(1 + \frac{\mathbf{k}_1 \cdot \mathbf{k}_2}{k_1^2} \right) c_1^L(k_2) \\ & + \left(1 + \frac{\mathbf{k}_1 \cdot \mathbf{k}_2}{k_2^2} \right) c_1^L(k_1) + c_2^L(\mathbf{k}_1, \mathbf{k}_2) \end{aligned} \quad (10)$$

where

$$F_2(\mathbf{k}_1, \mathbf{k}_2) = \frac{10}{7} + \left(\frac{k_1}{k_2} + \frac{k_2}{k_1} \right) \frac{\mathbf{k}_1 \cdot \mathbf{k}_2}{k_1 k_2} + \frac{4}{7} \left(\frac{\mathbf{k}_1 \cdot \mathbf{k}_2}{k_1 k_2} \right)^2, \quad (11)$$

is the second-order kernel of the Eulerian perturbation theory [38]. In the literature, an extra factor of $1/2!$ is frequently multiplied to the right-hand side of Eq. (11). We find it is convenient not to include the factor for symmetrical reasons in diagrammatic methods [1].

In the lowest-order approximation, non-Gaussian contributions to the renormalized bias functions can be neglected as described earlier. Consequently, we can consider that the first term of right-hand side of Eq. (2) corresponds to the Gaussian part $P_X^G(k)$ and the second term corresponds to the non-Gaussian part $\Delta P_X(k)$:

$$P_X^G(k) = [\Gamma_X^{(1)}(\mathbf{k})]^2 P_L(k), \quad (12)$$

$$\begin{aligned} \Delta P_X(k) = & \Gamma_X^{(1)}(\mathbf{k}) \int \frac{d^3k_1}{(2\pi)^3} \frac{d^3k_2}{(2\pi)^3} (2\pi)^3 \delta_D(\mathbf{k}_1 + \mathbf{k}_2 - \mathbf{k}) \\ & \times \Gamma_X^{(2)}(\mathbf{k}_1, \mathbf{k}_2) B_L(k, k_1, k_2). \end{aligned} \quad (13)$$

One should note that the above distinction holds only in the lowest-order approximation. In general, there are non-Gaussian corrections to the first multipoint propagator $\Gamma_X^{(1)}$ beyond the lowest-order approximation. Those corrections in Eq. (12) should be included in $\Delta P_X(k)$ if we consider the higher-order approximations. For example, the lowest-order non-Gaussian correction term is proportional to the primordial bispectrum. However, such correction terms are multiplied by the power spectrum in Eq. (12). Accordingly, the orders of non-Gaussian corrections to the multipoint propagator in Eq. (12) are higher than those of Eq. (13), and can be neglected in the lowest-order approximation. For the same reason, we do not consider loop corrections to the Gaussian

part $P_X^G(k)$ which are extensively studied in previous papers [36, 39–41] with Gaussian initial conditions. Evaluations of the leading non-Gaussian part $\Delta P_X(k)$ is the main subject in this paper.

Substituting Eqs. (9) and (10) into Eqs. (12) and (13) we have

$$P_X^G(k) = [b_1(k)]^2 P_L(k), \quad (14)$$

$$\Delta P_X(k) = b_1(k) [Q_0(k) + Q_1(k) + Q_2(k)], \quad (15)$$

where

$$b_1(k) = 1 + c_1^L(k) \quad (16)$$

corresponds to the Eulerian linear bias factor, and the functions $Q_n(k)$ are defined by

$$Q_n(k) = \int \frac{d^3 k'}{(2\pi)^3} \hat{Q}_n(\mathbf{k}, \mathbf{k}') B_L(k, k', |\mathbf{k} - \mathbf{k}'|), \quad (17)$$

where

$$\hat{Q}_0(\mathbf{k}, \mathbf{k}') = \frac{2\mathbf{k} \cdot \mathbf{k}'}{k'^2} - \frac{4}{7} \frac{k^2 k'^2 - (\mathbf{k} \cdot \mathbf{k}')^2}{k'^2 |\mathbf{k} - \mathbf{k}'|^2}, \quad (18)$$

$$\hat{Q}_1(\mathbf{k}, \mathbf{k}') = \frac{2\mathbf{k} \cdot \mathbf{k}'}{k'^2} c_1^L(|\mathbf{k} - \mathbf{k}'|), \quad (19)$$

$$\hat{Q}_2(\mathbf{k}, \mathbf{k}') = c_2^L(k', \mathbf{k} - \mathbf{k}'). \quad (20)$$

When the bias is local, the linear bias factor $b_1(k)$ is scale-independent. In general, the scale-dependent bias emerges from nonlocality even when the primordial non-Gaussianity is absent.

When the scale-dependent bias $\Delta b(k)$ from the primordial non-Gaussianity is defined by

$$P_X(k) = [b_1(k) + \Delta b(k)]^2 P_m(k), \quad (21)$$

and higher orders of Δb are neglected, we have

$$\Delta b(k) = \frac{1}{2} b_1(k) \left(\frac{\Delta P_X(k)}{P_X^G(k)} - \frac{\Delta P_m(k)}{P_m^G(k)} \right), \quad (22)$$

where $P_m^G(k)$ is the power spectrum of mass without primordial non-Gaussianity and $\Delta P_m(k)$ is the contribution from the primordial non-Gaussianity, so that $P_m(k) = P_m^G(k) + \Delta P_m(k)$ is the total power spectrum of mass. These are given by substituting $c_1^L = c_2^L = 0$ ($b_1 = 1$) in the expressions of $P_X^G(k)$ and $\Delta P_X(k)$, respectively:

$$P_m^G(k) = P_L(k), \quad (23)$$

$$\Delta P_m(k) = Q_0(k). \quad (24)$$

Substituting Eqs. (14), (15), (23) and (24) into Eq. (22), we have

$$\Delta b(k) = \frac{1}{2P_L(k)} [Q_1(k) + Q_2(k) - c_1^L(k)Q_0(k)]. \quad (25)$$

The above expression for the scale-dependent bias is consistent to that derived from the cross power spectrum $P_{mX}(k)$

between mass and objects X as shown below. In fact, the cross power spectrum is given by

$$\begin{aligned} P_{mX}(k) &= \Gamma_m^{(1)}(\mathbf{k}) \Gamma_X^{(1)}(\mathbf{k}) P_L(k) \\ &+ \frac{1}{2} \Gamma_m^{(1)}(\mathbf{k}) \int \frac{d^3 k'}{(2\pi)^3} \Gamma_X^{(2)}(\mathbf{k}', \mathbf{k} - \mathbf{k}') B_L(k, k', |\mathbf{k} - \mathbf{k}'|) \\ &+ \frac{1}{2} \Gamma_X^{(1)}(\mathbf{k}) \int \frac{d^3 k'}{(2\pi)^3} \Gamma_m^{(2)}(\mathbf{k}', \mathbf{k} - \mathbf{k}') B_L(k, k', |\mathbf{k} - \mathbf{k}'|) \\ &+ \dots, \end{aligned} \quad (26)$$

where $\Gamma_m^{(n)}$ is the n th multipoint propagator of mass. In the lowest-order approximation, the first two propagators are obtained by substituting $c_1^L = c_2^L = 0$ in Eqs. (9) and (10):

$$\Gamma_m^{(1)}(\mathbf{k}) = 1, \quad (27)$$

$$\Gamma_m^{(2)}(\mathbf{k}_1, \mathbf{k}_2) = F_2(\mathbf{k}_1, \mathbf{k}_2). \quad (28)$$

Substituting Eqs. (9), (10), (27) and (28) into Eq. (26), we have

$$P_{mX}^G(k) = b_1(k) P_L(k), \quad (29)$$

$$\Delta P_{mX}(k) = \frac{1 + b_1(k)}{2} Q_0(k) + \frac{1}{2} Q_1(k) + \frac{1}{2} Q_2(k). \quad (30)$$

When the scale-dependent bias $\Delta b(k)$ is defined by

$$P_{mX}(k) = [b_1(k) + \Delta b(k)] P_m(k), \quad (31)$$

and higher orders of Δb are neglected, we have

$$\Delta b(k) = b_1(k) \left(\frac{\Delta P_{mX}(k)}{P_{mX}^G(k)} - \frac{\Delta P_m(k)}{P_m^G(k)} \right). \quad (32)$$

Substituting Eqs. (23), (24), (29) and (30) into Eq. (32), we again have the same equation as Eq. (25).

Our result, Eq. (25), is a general formula and any approximation other than the perturbation theory is not employed. In the literature, analytic formulas of scale-dependent bias from the primordial non-Gaussianity have been derived either in the high-peak limit or in the approximation of peak-background split. These approximate results are subclasses of our general formula, as we explicitly show in the rest of this paper.

III. MODELS OF PRIMORDIAL NON-GAUSSIANITY

A. Specific models of primordial bispectra

Models of primordial non-Gaussianity are quite commonly characterized by the primordial bispectra B_Φ of gauge-invariant Newtonian potential Φ at the matter-dominated epoch. The linear density contrast δ_L is proportional to Φ in Fourier space, and we have

$$\delta_L(\mathbf{k}) = \mathcal{M}(k) \Phi(\mathbf{k}). \quad (33)$$

Throughout this paper, we do not explicitly write an argument of time or redshift z for simplicity in some time-dependent

variables. In the above equation, $\delta_L \propto D(z)$ and $\mathcal{M} \propto D(z)$ where $D(z)$ is the linear growth factor. However, the potential Φ is the primordial one and does not depend on z by definition. Do not confuse with the physical Newtonian potential which does depend on z . The proportional factor $\mathcal{M}(k)$ is determined by the transfer function $T(k)$ and the Poisson equation as

$$\mathcal{M}(k) = \frac{2}{3} \frac{D(z)}{(1+z_*)D(z_*)} \frac{k^2 T(k)}{H_0^2 \Omega_{m0}}, \quad (34)$$

where z_* is an arbitrary redshift at the matter-dominated epoch. The factor $(1+z_*)D(z_*)$ does not depend on the choice of z_* as long as z_* is deep in the matter-dominated epoch, since $D(z_*) \propto 1/(1+z_*)$ in that epoch. Some authors employ the normalization of the growth factor as $(1+z_*)D(z_*) = 1$, in which case Eq. (34) has the simplest form.

The linear power spectrum and bispectrum of δ_L are given by

$$P_L(k) = \mathcal{M}^2(k) P_\Phi(k) \quad (35)$$

$$B_L(k_1, k_2, k_3) = \mathcal{M}(k_1) \mathcal{M}(k_2) \mathcal{M}(k_3) B_\Phi(k_1, k_2, k_3), \quad (36)$$

where $P_\Phi(k)$ and $B_\Phi(k_1, k_2, k_3)$ are the primordial power spectrum and bispectrum of the potential, respectively. In popular models of non-Gaussianity, the primordial bispectra are uniquely related to the shape of primordial power spectrum.

There are four models of primordial bispectra which are frequently considered as typical examples. Defining

$$P_i \equiv P_\Phi(k_i), \quad (37)$$

the four models are given by the following equations:

- the *local* model [42–44]:

$$B_\Phi^{\text{loc.}}(k_1, k_2, k_3) = 2f_{\text{NL}} [P_1 P_2 + \text{cyc.}]. \quad (38)$$

- the *equilateral* model [45]:

$$B_\Phi^{\text{eq.}}(k_1, k_2, k_3) = 6f_{\text{NL}} \left[-(P_1 P_2 + \text{cyc.}) - 2(P_1 P_2 P_3)^{2/3} + (P_1^{1/3} P_2^{2/3} P_3 + 5 \text{ perm.}) \right]. \quad (39)$$

- the *folded* model [46]:

$$B_\Phi^{\text{fol.}}(k_1, k_2, k_3) = 6f_{\text{NL}} \left[(P_1 P_2 + \text{cyc.}) + 3(P_1 P_2 P_3)^{2/3} - (P_1^{1/3} P_2^{2/3} P_3 + 5 \text{ perm.}) \right]. \quad (40)$$

- the *orthogonal* model [47]:

$$B_\Phi^{\text{ort.}}(k_1, k_2, k_3) = 6f_{\text{NL}} \left[-3(P_1 P_2 + \text{cyc.}) - 8(P_1 P_2 P_3)^{2/3} + 3(P_1^{1/3} P_2^{2/3} P_3 + 5 \text{ perm.}) \right]. \quad (41)$$

With these typical models of primordial bispectrum, the linear bispectrum $B_L(k_1, k_2, k_3)$ is given by the linear power spectrum $P_L(k)$ and a function $\mathcal{M}(k)$ through Eqs. (35) and (36). Once a model of the primordial non-Gaussianity is given, the non-Gaussian part of the power spectrum $\Delta P_X(k)$, $\Delta P_{\text{mX}}(k)$, $\Delta P_{\text{m}}(k)$ of Eqs. (15), (30), (24) and the scale-dependent bias of Eq. (25) are straightforwardly evaluated for a given model of bias functions.

B. Large-scale limit of scale-dependent bias

In the large-scale limit $k \rightarrow 0$ of Eq. (17), we have $\hat{Q}_0(\mathbf{k}, \mathbf{k}') \approx \hat{Q}_1(\mathbf{k}, \mathbf{k}') \approx 0$ in Eqs. (18) and (19). Accordingly, we have $Q_0(k) \approx Q_1(k) \approx 0$, and the scale-dependent bias of Eq. (25) approximately reduces to

$$\Delta b(k) \approx \frac{Q_2(k)}{2P_L(k)}. \quad (42)$$

As long as the second-order renormalized bias function $c_2^L(\mathbf{k}_1, \mathbf{k}_2)$ is a smooth function, we can adopt an approximation

$$c_2^L(\mathbf{k}', \mathbf{k} - \mathbf{k}') \approx c_2^L(\mathbf{k}', -\mathbf{k}') \quad (43)$$

in the large-scale limit for the integrand of $Q_2(k)$. Because of rotational symmetry, $c_2^L(\mathbf{k}', -\mathbf{k}')$ only depends on the magnitude $k' = |\mathbf{k}'|$, and we define

$$\tilde{c}_2^L(k') \equiv c_2^L(\mathbf{k}', -\mathbf{k}'). \quad (44)$$

Assuming Eq. (43) for the renormalized bias function, the scale-dependent bias on large scales is asymptotically given by

$$\Delta b(k) \approx \frac{1}{2P_L(k)} \int \frac{d^3 k'}{(2\pi)^3} \tilde{c}_2^L(k') B_L(k, k', |\mathbf{k} - \mathbf{k}'|). \quad (45)$$

In this case, the scale dependence of $\Delta b(k)$ is determined by the functional form of the primordial bispectrum $B_L(k, k', |\mathbf{k} - \mathbf{k}'|)$ in the squeezed limit $k \ll k'$.

For specific models of primordial non-Gaussianity introduced in the previous subsection, squeezed limits of the bispectra can be analytically derived. In the following, we assume the power-law primordial spectrum, $P_\Phi(k) \propto k^{n_s-4}$, where $n_s \approx 1$ is the scalar spectral index. We define

$$\alpha_s = \frac{1 - n_s}{3}, \quad (46)$$

to represent the deviation from the scale-free Harrison-Zel'dovich spectrum, $n_s = 1$. Taking the squeezed limit $k \ll k'$ in Eqs. (38)–(41), and keeping leading orders in k/k' , they are asymptotically given by

$$B_\Phi^{\text{loc.}}(k, k', |\mathbf{k} - \mathbf{k}'|) \approx 4f_{\text{NL}} P_\Phi(k) P_\Phi(k'), \quad (47)$$

$$B_\Phi^{\text{eq.}}(k, k', |\mathbf{k} - \mathbf{k}'|) \approx 12f_{\text{NL}} \left(\frac{k}{k'} \right)^2 \left[\left(\frac{k}{k'} \right)^{2\alpha_s} - (1 + \alpha_s)^2 \mu^2 \right] \times P_\Phi(k) P_\Phi(k'), \quad (48)$$

$$B_\Phi^{\text{fol.}}(k, k', |\mathbf{k} - \mathbf{k}'|) \approx 6f_{\text{NL}} \frac{k}{k'} P_\Phi(k) P_\Phi(k'), \quad (49)$$

$$B_\Phi^{\text{ort.}}(k, k', |\mathbf{k} - \mathbf{k}'|) \approx -12f_{\text{NL}} \frac{k}{k'} P_\Phi(k) P_\Phi(k'), \quad (50)$$

where $\mu \equiv \mathbf{k} \cdot \mathbf{k}' / kk'$ is the direction cosine between wavevectors \mathbf{k} and \mathbf{k}' . Except for the equilateral non-Gaussianity, the lowest-order bispectra divided by $P_\Phi(k) P_\Phi(k')$ in the squeezed limit do not have explicit dependences on α_s .

Substituting Eqs. (47)–(50) into Eqs. (36) and (45), we have

$$\Delta b^{\text{loc.}}(k) \approx \frac{2f_{\text{NL}}}{\mathcal{M}(k)} \int \frac{d^3k'}{(2\pi)^3} \tilde{c}_2^{\text{L}}(k') P_{\text{L}}(k'), \quad (51)$$

$$\Delta b^{\text{eq.}}(k) \approx \frac{6f_{\text{NL}}k^2}{\mathcal{M}(k)} \left[k^{2\alpha_s} \int \frac{d^3k'}{(2\pi)^3} \frac{\tilde{c}_2^{\text{L}}(k')}{k'^{2(1+\alpha_s)}} P_{\text{L}}(k') \right. \\ \left. - \frac{(1+\alpha_s)^2}{3} \int \frac{d^3k'}{(2\pi)^3} \frac{\tilde{c}_2^{\text{L}}(k')}{k'^2} P_{\text{L}}(k') \right] \quad (52)$$

$$\Delta b^{\text{fol.}}(k) \approx \frac{3f_{\text{NL}}k}{\mathcal{M}(k)} \int \frac{d^3k'}{(2\pi)^3} \frac{\tilde{c}_2^{\text{L}}(k')}{k'} P_{\text{L}}(k'), \quad (53)$$

$$\Delta b^{\text{ort.}}(k) \approx -\frac{6f_{\text{NL}}k}{\mathcal{M}(k)} \int \frac{d^3k'}{(2\pi)^3} \frac{\tilde{c}_2^{\text{L}}(k')}{k'} P_{\text{L}}(k'), \quad (54)$$

respectively. To derive the above equations, we use an approximation $\mathcal{M}(|\mathbf{k} - \mathbf{k}'|) \approx \mathcal{M}(k')$ in the squeezed limit. In the case of equilateral non-Gaussianity, the asymptote of Eq. (52) is somehow complicated for a general value of the spectral index n_s . In the case of scale-free spectrum, $n_s = 1$ ($\alpha_s = 0$), Eq. (52) reduces to a simpler form,

$$\Delta b^{\text{eq.}}(k) \approx \frac{4f_{\text{NL}}k^2}{\mathcal{M}(k)} \int \frac{d^3k'}{(2\pi)^3} \frac{\tilde{c}_2^{\text{L}}(k')}{k'^2} P_{\text{L}}(k'), \quad (n_s = 1). \quad (55)$$

The integrals in Eqs. (51)–(55) do not depend on k . Consequently, only the amplitudes of the scale-dependent bias $\Delta b(k)$ are sensitive to details of biasing in the large-scale limit. The scaling indices are sensitive to only the primordial bispectra, and are independent on details of biasing. On sufficiently large scales, where $T(k) \approx 1$ and $\mathcal{M}(k) \propto k^{-2}$, the known scalings

$$\Delta b^{\text{loc.}} \propto k^{-2}, \quad (56)$$

$$\Delta b^{\text{eq.}} \propto k^0, \quad (57)$$

$$\Delta b^{\text{fol.}} \propto k^{-1}, \quad (58)$$

$$\Delta b^{\text{ort.}} \propto k^{-1} \quad (59)$$

hold irrespective to bias models. The scale-independence in the case of equilateral model holds only for the scale-free power spectrum, $n_s = 1$. The above scalings are derived in the literature for individual models of biasing, such as the halo model with peak-background split [15], the high-peak model [19], and the local bias model [22]. Our general argument here shows that those scalings are general consequences of squeezed limits of primordial bispectra, and are independent on bias models. Only the proportional coefficients of Eqs. (56)–(59) depend on bias models. This finding explains why different models of bias in the literature give different amplitudes and the same spectral index of scale-dependent bias.

For a given model of primordial bispectrum, obtaining the value of scaling index of the scale-dependent bias in the large-scale limit is straightforward even if the bias model is not specified: the scaling index in that limit is just given by the squeezed limit of the primordial bispectrum through Eq. (45), i.e., the large-scale behavior of $\Delta b(k)$ as a function of k is determined by a combination $B_{\text{L}}(k, k', |\mathbf{k} - \mathbf{k}'|)/P_{\text{L}}(k)$ in the limit of $k \ll k'$. In the following sections, we look into the amplitudes which are determined by concrete forms of the renormalized bias function of second order, $c_2^{\text{L}}(\mathbf{k}_1, \mathbf{k}_2)$.

IV. SHAPES OF RENORMALIZED BIAS FUNCTIONS

Detailed amplitude and shape of scale-dependent bias depend on the form of renormalized bias functions c_n^{L} . In the lowest-order approximation of this paper, the first two functions, $c_1^{\text{L}}(\mathbf{k})$ and $c_2^{\text{L}}(\mathbf{k}_1, \mathbf{k}_2)$, are of primary interest. In this section, we derive the general form of renormalized bias functions c_n^{L} in the halo model of bias.

A. Asymptotes of the halo bias functions

The scale-dependent bias is previously derived in the halo approach with the method of peak-background split [5, 9, 15, 17]. With this method, it is shown that the lowest-order term in scale-dependent bias, which is proportional to f_{NL} , is proportional to the first-order Lagrangian bias parameter b_1^{L} . On the other hand, Eulerian local bias models predict the corresponding term is proportional to the second-order bias parameter b_2 [22]. Both predictions agree with each other in the high-peak limit, although the difference should be important in physically realistic situations. Numerical simulations indicate that the corresponding term is proportional to b_1^{L} , which agrees with the results of the peak-background split [16–18].

In our asymptotic prediction of Eq. (45), the corresponding term is related to the second-order renormalized bias function, c_2^{L} . Does that mean our prediction contradicts with the prediction of the peak-background split in the halo model? As we shall see below, the answer is no. To see the relation between our general results and the prediction of peak-background split, one needs to derive the scale-dependence of the function $c_2^{\text{L}}(\mathbf{k}_1, \mathbf{k}_2)$ in the model of halo bias.

First we introduce our notations of the halo approach. In the halo model, the mass M of halo is related to the Lagrangian radius R of a spherical cell by

$$M = \frac{4}{3}\pi\bar{\rho}_0 R^3, \quad (60)$$

where $\bar{\rho}_0$ is the mean matter density at the present time, or

$$R = \left[\frac{M}{1.162 \times 10^{12} h^{-1} M_{\odot} \Omega_{\text{m}0}} \right]^{1/3}, \quad (61)$$

where $M_{\odot} = 1.989 \times 10^{30}$ kg is the mass of the sun. In the following, the radius R is always a function of a mass scale M through the above equation. The density variance of mass scale M is given by

$$\sigma_M^2 = \int \frac{d^3k}{(2\pi)^3} W^2(kR) P_{\text{L}}(k), \quad (62)$$

where the function $W(kR)$ is usually chosen to be a top-hat window function,

$$W(x) = \frac{3j_1(x)}{x} = \frac{3 \sin x - 3x \cos x}{x^3}, \quad (63)$$

and $j_1(x)$ is the first-order spherical Bessel function.

In Ref. [1], the large-scale asymptotes of the bias functions are derived in the halo approach with a universal mass function. The mass function is said to be universal when the mass function has a form

$$n(M)dM = \frac{\bar{\rho}_0}{M} f_{\text{MF}}(\nu) \frac{d\nu}{\nu}, \quad (64)$$

where $\nu = \delta_c/\sigma_M$ is a function of mass M , and δ_c is the critical overdensity for spherical collapse. In the Einstein-de Sitter model, the critical overdensity is exactly independent of redshift, $\delta_c = 3(3\pi/2)^{2/3}/5 \simeq 1.686$, while it only weakly depends on cosmological parameters and redshift in general cosmology. The multiplicity function $f_{\text{MF}}(\nu)$ has a normalization

$$\int_0^\infty f_{\text{MF}}(\nu) \frac{d\nu}{\nu} = 1 \quad (65)$$

to ensure all the mass in the universe is to be contained in halos.

In the literature, several forms of the multiplicity function f_{MF} are proposed. In the original Press-Schechter (PS) theory [48], it has a form,

$$f_{\text{PS}}(\nu) = \sqrt{\frac{2}{\pi}} \nu e^{-\nu^2/2}. \quad (66)$$

Sheth and Tormen (ST) [49] give a better fit to numerical simulations of cold-dark-matter type cosmologies with Gaussian initial conditions,

$$f_{\text{ST}}(\nu) = A(p) \sqrt{\frac{2}{\pi}} \left[1 + \frac{1}{(q\nu^2)^p} \right] \sqrt{q} \nu e^{-q\nu^2/2}, \quad (67)$$

where $p = 0.3$, $q = 0.707$ are numerically fitted parameters, and $A(p) = [1 + \pi^{-1/2} 2^{-p} \Gamma(1/2 - p)]^{-1}$ is the normalization factor. When $p = 0$, $q = 1$, the ST mass function reduces to the PS mass function.

Several other fitting formulas for f_{MF} have been proposed with numerically improved calibrations [50–52]. In Warren et al. [51], for example, the multiplicity function is fitted as a function of $\sigma \equiv \sigma_M$ instead of ν as

$$\tilde{f}_{\text{W}}(\sigma) = A (\sigma^{-a} + b) \exp\left(-\frac{c}{\sigma^2}\right), \quad (68)$$

where A, a, b, c are fitting parameters. The same functional form is applied to MICE simulations in Ref. [52], allowing the parameters redshift-dependent. Their values are given by $A(z) = 0.58(1+z)^{-0.13}$, $a(z) = 1.37(1+z)^{-0.15}$, $b(z) = 0.3(1+z)^{-0.084}$, $c(z) = 1.036(1+z)^{-0.024}$. As a function of ν , Eq. (68) can be re-expressed as

$$f_{\text{W}}(\nu) = \tilde{f}_{\text{W}}(\delta_c/\nu) = A \left[\left(\frac{\nu}{\delta_c} \right)^a + b \right] \exp\left(-\frac{c\nu^2}{\delta_c^2}\right). \quad (69)$$

In the following, we refer to the above form as “MICE mass function” when the redshift-dependent parameters with MICE simulations are adopted. When the parameters A, a, b, c are redshift-dependent as in the case of MICE simulations, the

multiplicity function explicitly depends on the redshift as $f_{\text{MF}}(\nu, z)$. In this case, the mass function is not universal anymore. Throughout this paper, explicit dependences on time is notationally suppressed in the arguments of functions, and we adopt the notation $f_{\text{MF}}(\nu)$ even if this function explicitly depends on the redshift. The PS mass function is recovered when we formally substitute $A = \sqrt{2/\pi} \delta_c$, $a = 1$, $b = 0$, $c = \delta_c^2/2$ into Eq. (69).

Using the notations introduced above, the long-wavelength asymptotes of the bias functions derived in Ref. [1] have the form,

$$c_n^{\text{L}}(\mathbf{k}_1, \dots, \mathbf{k}_n) \approx b_n^{\text{L}}(M) \quad (|\mathbf{k}_i| \rightarrow 0), \quad (70)$$

where $b_n^{\text{L}}(M)$ is a scale-independent function defined by

$$b_n^{\text{L}}(M) = \left(-\frac{1}{\sigma_M} \right)^n \frac{f_{\text{MF}}^{(n)}(\nu)}{f_{\text{MF}}(\nu)}, \quad (71)$$

and $f_{\text{MF}}^{(n)} = d^n f_{\text{MF}}/d\nu^n$ denotes n th derivative with respect to ν .

Specifically, when the PS mass function with Eq. (66) is applied, we have

$$b_1^{\text{L}}(M) = \frac{\nu^2 - 1}{\delta_c}, \quad b_2^{\text{L}}(M) = \frac{\nu^4 - 3\nu^2}{\delta_c^2}, \quad (72)$$

and so forth, which are consistent with the results derived from the model of spherical collapse [53, 54]. When the ST mass function with Eq. (67) is applied, we have

$$b_1^{\text{L}}(M) = \frac{1}{\delta_c} \left[q\nu^2 - 1 + \frac{2p}{1 + (q\nu^2)^p} \right], \quad (73)$$

$$b_2^{\text{L}}(M) = \frac{1}{\delta_c^2} \left[q^2\nu^4 - 3q\nu^2 + \frac{2p(2q\nu^2 + 2p - 1)}{1 + (q\nu^2)^p} \right], \quad (74)$$

and so forth. When the MICE mass function with Eq. (68) is applied, we have

$$b_1^{\text{L}}(M) = \frac{1}{\delta_c} \left(\frac{2c}{\sigma^2} - \frac{a}{1 + b\sigma^a} \right), \quad (75)$$

$$b_2^{\text{L}}(M) = \frac{1}{\delta_c^2} \left[\frac{4c^2}{\sigma^4} - \frac{2c}{\sigma^2} - \frac{a(4c/\sigma^2 - a + 1)}{1 + b\sigma^a} \right], \quad (76)$$

and so forth, where $\sigma = \sigma_M = \delta_c/\nu$. The bias parameters $b_1^{\text{L}}(M)$ and $b_2^{\text{L}}(M)$ as functions of mass are plotted in Fig. 3 for three different mass functions considered above.

If the asymptotes of Eq. (70) are naively used in Eq. (45), the scale-dependent bias is proportional to the second-order Lagrangian bias parameter $\Delta b \propto b_2^{\text{L}}$. Bias parameters are scale-independent in models of local bias. Therefore, the use of asymptotes of Eq. (70) restrict ourselves to a model of local bias. Local bias models predict that the scale-dependent bias Δb is proportional to the second-order bias parameter b_2 in general [22]. One should note that when c_2^{L} is exactly constant, the integral in Eq. (51) logarithmically diverges for the local model of primordial non-Gaussianity with a cold-dark-matter type power spectrum which has a small-scale asymptote $P_{\text{L}}(k) \propto k^{-3}$ for $k \rightarrow \infty$.

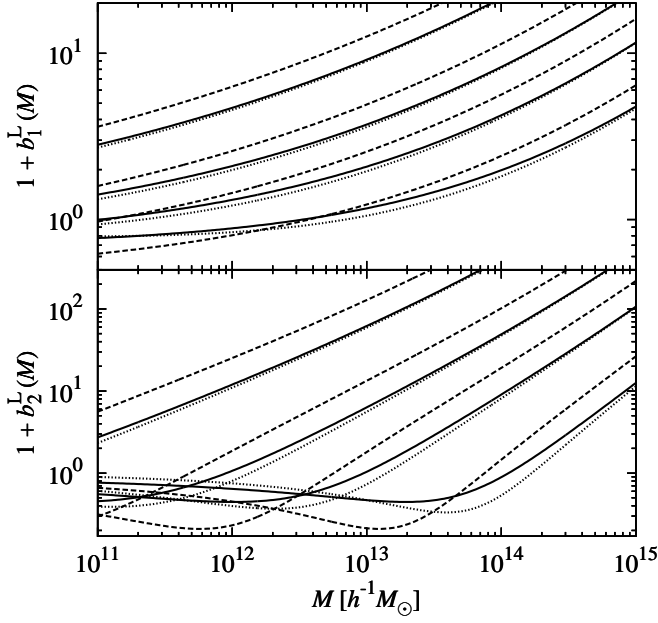


FIG. 3: The scale-independent Lagrangian bias parameters derived from the Sheth-Tormen (solid lines), Press-Schechter (dashed lines) and MICE (dotted lines) mass functions for $z = 0, 1, 2, 4$ (from bottom to top on large mass scales). The unity is added to each parameter to show the negative values in this logarithmic plot.

The local bias model turned out *not* to be a good approximation in modeling the scale-dependent bias of halos measured in numerical simulations with non-Gaussian initial conditions [14, 16, 18]. The scale-dependent bias is more or less proportional to the first-order bias parameter $\Delta b \propto b_1^L$ rather than the second-order parameter b_2^L . The property $\Delta b \propto b_1^L$ is a general prediction of the halo approach with the method of peak-background split [5, 9, 15]. That means the method of peak-background split takes into account the nonlocal nature of biasing. The fact that the predictions of the peak-background split are better than those of local bias model in reproducing the results of numerical simulations implies that nonlocal nature of biasing is important to understand the scale-dependent bias from the primordial non-Gaussianity.

B. Renormalized bias functions of halos without assuming peak-background split

In the following several subsections, we extend the calculation of the renormalized bias functions beyond the asymptotic limit of Eq. (70), without resorting to the approximation of peak-background split. In the end, the known formula of scale-dependent bias derived from the peak-background split is exactly re-derived as limiting cases, which is one of the remarkable findings in this paper.

In the literature, analytic formulas of halo bias are derived by more or less adopting a concept of peak-background split. This method is necessary because the halo approach is based on a statistical nature of extended Press-Schechter mass func-

tion. In such an approach, the local mass function is obtained by averaging over small-scale fluctuations, while large-scale fluctuations are considered as background modulation field, which leads spatial fluctuations of number density of halos. Comparing the fluctuations of the halo number density field and those of mass, the halo bias is analytically derived.

However, the biasing can be seen as a deterministic process at a most fundamental level, in which any statistical information is not required. One can think of getting a halo catalog in numerical simulations to understand the situation. Just one realization of the initial condition deterministically gives subsequent nonlinear evolutions and formation sites of halos.

When only leading growing modes are considered in a perturbation theory, any structure in the universe is deterministically related to the linear density field. The biasing relation should not require statistical information of the field. In calculating the renormalized bias functions of Eq. (3), the number density fluctuations δ_X^L is a deterministic functional of linear density field δ_L . Any statistical quantities, such as the short-mode power spectrum in the method of peak-background split, are not expected to appear at the most fundamental level.

From considerations above, we start from an unaveraged version of the original Press-Schechter (PS) formalism [48]. The linear density field smoothed over mass scale M ,

$$\delta_M(\mathbf{x}) = \int \frac{d^3k}{(2\pi)^3} e^{ik \cdot \mathbf{x}} W(kR) \delta_L(\mathbf{k}), \quad (77)$$

is a fundamental element in the original PS formalism and its variants. When $P(M, \delta_c)$ denotes the probability that (or the volume fraction where) the value δ_M exceeds a critical value δ_c , the averaged number density of halos in the original PS formalism are given by

$$n(M) = -\frac{2\bar{\rho}_0}{M} \frac{\partial}{\partial M} P(M, \delta_c), \quad (78)$$

where $n(M)$ is the *differential* mass function. In some literatures, $n(M)$ is denoted by dn/dM , which notation we do not adopt. When the distribution function of δ_M is exactly Gaussian, Eq. (78) is equivalent to Eq. (64) with Eq. (66).

For our purpose, we need to have a local number density of halos $n(\mathbf{x}, M)$, instead of spatially averaged one. The condition that a mass element at a particular point is included in a collapsed halo of mass greater than M is not stochastic but deterministic when the linear density field is given. Consequently, localized version of Eq. (78) should be

$$n(\mathbf{x}, M) = -\frac{2\bar{\rho}_0}{M} \frac{\partial}{\partial M} \Theta[\delta_M(\mathbf{x}) - \delta_c], \quad (79)$$

where $\Theta(x)$ is a step function, and \mathbf{x} is a Lagrangian position. The statistical quantities do not appear in this relation. For a given realization of linear density field δ_L , the mass element at a given point is either collapsed $\delta_M > \delta_c$ or uncollapsed $\delta_M < \delta_c$. Taking the spatial average of Eq. (79), Eq. (78) of the original PS formalism follows, because

$$\langle \Theta(\delta_M(\mathbf{x}) - \delta_c) \rangle = P(M, \delta_c). \quad (80)$$

In a picture of excursion set approach [55], the step function in Eq. (79) should be replaced by an operator $N_{\text{up}}(M)$, which is zero until the first up-crossing $\delta_M > \delta_c$ occurs as the mass scale M decreases from infinity, and it becomes unity below that mass scale. This operator N_{up} is not just a single function of δ_M , and analytic treatments are more complicated if not impossible. In this paper, we just use Eq. (79) in the following consideration for simplicity.

It is also possible to consider the function Θ is a general function which is not necessarily a step function. When this function is a step function, the PS mass function exactly follows when the linear density field is random Gaussian and the model of spherical collapse is literally assumed. However, in reality, the mass function is different from the PS one even if the linear density field is random Gaussian. In approaches of universal mass function, the step function is deformed to a different function to reproduce a mass function $n(M)$ in numerical simulations. We allow this possibility and the function Θ is not necessarily a step function in the following derivation.

The number density contrast in Lagrangian space is given by $\delta_h^L(\mathbf{x}) = n(\mathbf{x}, M)/n(M) - 1$ for halos of mass M , where Eqs. (78) and (79) are assumed. Taking functional derivatives of Eq. (79), we have

$$\frac{\delta^n n(\mathbf{x}, M)}{\delta \delta_L(\mathbf{k}_1) \cdots \delta \delta_L(\mathbf{k}_n)} = -\frac{e^{i(\mathbf{k}_1 + \cdots + \mathbf{k}_n) \cdot \mathbf{x}}}{(2\pi)^{3n}} \frac{2\bar{\rho}_0}{M} \times \frac{\partial}{\partial M} \left[\Theta^{(n)}(\delta_M - \delta_c) W(k_1 R) \cdots W(k_n R) \right], \quad (81)$$

where Eq. (77) is used and $\Theta^{(n)}(x) = d^n \Theta(x)/dx^n$. Fourier transforming the above equation with respect to \mathbf{x} and taking ensemble average, the renormalized bias functions of Eq. (3) or Eq. (4) reduce to

$$c_n^L(\mathbf{k}_1, \dots, \mathbf{k}_n) = \frac{(-1)^n \frac{\partial}{\partial M} \left[\frac{\partial^n P(M, \delta_c)}{\partial \delta_c^n} W(k_1 R) \cdots W(k_n R) \right]}{\frac{\partial P(M, \delta_c)}{\partial M}}, \quad (82)$$

where R is an explicit function of M and partial derivatives of the window functions with respect to M do not vanish.

C. Renormalized bias functions in universal mass functions

Assuming a universal mass function of Eq. (64), we have a form

$$P(M, \delta_c) = \frac{1}{2} F(\nu), \quad (83)$$

where

$$F(\nu) \equiv \int_{\nu}^{\infty} \frac{f_{\text{MF}}(\nu)}{\nu} d\nu, \quad (84)$$

is a filling factor of collapsed regions. Partial derivatives in Eq. (82) are given by

$$\frac{\partial P(M, \delta_c)}{\partial M} = \frac{f_{\text{MF}}(\nu)}{2} \frac{d \ln \sigma_M}{dM}, \quad (85)$$

$$\frac{\partial^n P(M, \delta_c)}{\partial \delta_c^n} = \frac{F^{(n)}(\nu)}{2\sigma_M^n}, \quad (86)$$

where

$$\begin{aligned} F^{(n)}(\nu) &= \frac{d^n F}{d\nu^n} = -\frac{d^{n-1}}{d\nu^{n-1}} \left[\frac{f_{\text{MF}}(\nu)}{\nu} \right] \\ &= \frac{(-1)^n (n-1)!}{\nu^n} \sum_{j=0}^{n-1} \frac{(-1)^j}{j!} \nu^j f_{\text{MF}}^{(j)}(\nu). \end{aligned} \quad (87)$$

In this case, Eq. (82) reduces to

$$c_n^L(\mathbf{k}_1, \dots, \mathbf{k}_n) = \frac{(-1)^n}{f_{\text{MF}}(\nu)} \frac{d}{d \ln \sigma_M} \left[\frac{F^{(n)}(\nu) W(k_1 R) \cdots W(k_n R)}{\sigma_M^n} \right]. \quad (88)$$

To evaluate the above expression, we have useful formulas,

$$\frac{dF^{(n)}(\nu)}{d \ln \sigma_M} = -\nu F^{(n+1)} = \frac{(-1)^n n!}{\nu^n} \sum_{j=0}^n \frac{(-1)^j}{j!} \nu^j f_{\text{MF}}^{(j)}, \quad (89)$$

$$\frac{d}{d \ln \sigma_M} \left(\frac{F^{(n)}(\nu)}{\sigma_M^n} \right) = \frac{1}{\sigma_M^n} \left[\frac{dF^{(n)}(\nu)}{d \ln \sigma_M} - n F^{(n)}(\nu) \right] = \frac{f_{\text{MF}}^{(n)}}{\sigma_M^n}. \quad (90)$$

One can use the scale-independent parameters $b_n^L(M) = (-1/\sigma_M)^n f_{\text{MF}}^{(n)}/f_{\text{MF}}$ introduced in Eq. (71) in the above equations. Accordingly, Eq. (88) reduces to two equivalent expressions,

$$\begin{aligned} c_n^L(\mathbf{k}_1, \dots, \mathbf{k}_n) &= \frac{A_n(M)}{\delta_c^n} W(k_1 R) \cdots W(k_n R) \\ &+ \frac{A_{n-1}(M) \sigma_M^n}{\delta_c^n} \frac{d}{d \ln \sigma_M} \left[\frac{W(k_1 R) \cdots W(k_n R)}{\sigma_M^n} \right], \end{aligned} \quad (91)$$

and

$$\begin{aligned} c_n^L(\mathbf{k}_1, \dots, \mathbf{k}_n) &= b_n^L(M) W(k_1 R) \cdots W(k_n R) \\ &+ \frac{A_{n-1}(M)}{\delta_c^n} \frac{d}{d \ln \sigma_M} [W(k_1 R) \cdots W(k_n R)]. \end{aligned} \quad (92)$$

where

$$A_n(M) \equiv \sum_{j=0}^n \frac{n!}{j!} \delta_c^j b_j^L(M). \quad (93)$$

and $b_0^L(M) \equiv 1$ for consistency. There is a recursion relation,

$$A_n = n A_{n-1} + \delta_c^n b_n^L, \quad (94)$$

which also guarantees the equivalence between the two expressions of Eqs. (91) and (92). In this paper, we need the

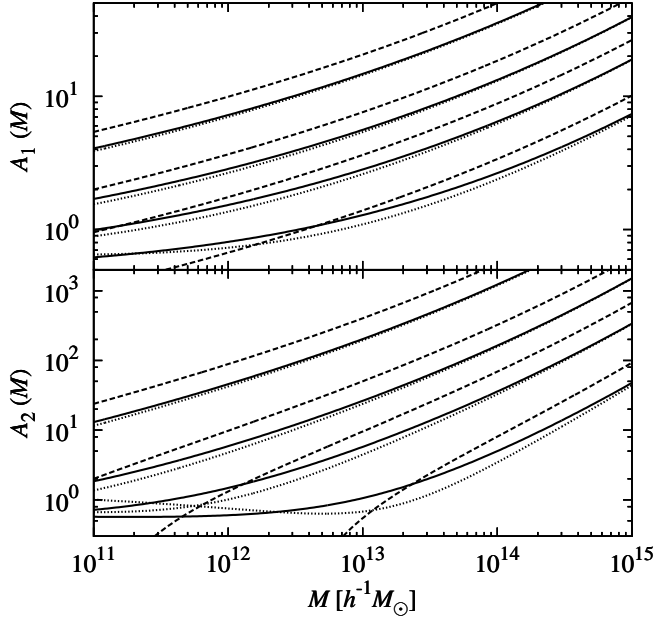


FIG. 4: The functions $A_1(M)$ and $A_2(M)$ derived from the Sheth-Tormen (solid lines), Press-Schechter (dashed lines) and MICE (dotted lines) mass functions for $z = 0, 1, 2, 4$ (from bottom to top on large mass scales).

renormalized bias functions up to second order. Explicitly, we have

$$A_0(M) = 1, \quad (95)$$

$$A_1(M) = 1 + \delta_c b_1^L(M), \quad (96)$$

$$A_2(M) = 2 + 2\delta_c b_1^L(M) + \delta_c^2 b_2^L(M). \quad (97)$$

The functions $A_1(M)$ and $A_2(M)$ are plotted in Fig. 4 for three kinds of mass functions considered in Sec. IV A.

When all the magnitudes of wavevector are small, $|\mathbf{k}_i| \rightarrow 0$, the window function becomes asymptotically unity, $W(k_i R) \rightarrow 1$. Accordingly, the previous result of Eq. (70) is correctly recovered in this limit. Therefore, Eq. (91) or Eq. (92) gives the form of renormalized bias functions beyond the approximation of large-scale limit. Scale-dependence of bias functions means nonlocality of the bias in general. The derived renormalized bias functions are scale-dependent on scales of mass M , which suggests that the halo bias is non-local on scales of halo mass, as naturally expected. Our formula, Eq. (91) or (92), can be used in general applications of iPT with the halo bias, beyond the problem of scale-dependent bias in this paper.

Up to the second order, we explicitly have

$$c_1^L(k) = b_1^L(M)W(kR) + \frac{1}{\delta_c} \frac{\partial W(kR)}{\partial \ln \sigma_M}, \quad (98)$$

$$c_2^L(\mathbf{k}_1, \mathbf{k}_2) = b_2^L(M)W(k_1 R)W(k_2 R) + \frac{1 + \delta_c b_1^L(M)}{\delta_c^2} \frac{\partial}{\partial \ln \sigma_M} [W(k_1 R)W(k_2 R)]. \quad (99)$$

The Eqs. (98) and (99) complete the elements to calculate our prediction for the scale-dependent bias, Eq. (25), in the case of halo bias. For convenience, we define

$$\mathcal{I}_n(k) = \int \frac{d^3 k'}{(2\pi)^3} \hat{\mathcal{I}}_n(\mathbf{k}, \mathbf{k}') B_L(k, k', |\mathbf{k} - \mathbf{k}'|), \quad (100)$$

for $n = 1, 2$, where

$$\hat{\mathcal{I}}_1(\mathbf{k}, \mathbf{k}') = \frac{2\mathbf{k} \cdot \mathbf{k}'}{k'^2} W(|\mathbf{k} - \mathbf{k}'|R), \quad (101)$$

$$\hat{\mathcal{I}}_2(\mathbf{k}, \mathbf{k}') = W(k'R)W(|\mathbf{k} - \mathbf{k}'|R). \quad (102)$$

When the bias functions are given by Eqs. (98) and (99), the functions $Q_1(k)$ and $Q_2(k)$ of Eqs. (17), (19), (20) are represented as

$$Q_1(k) = b_1^L \mathcal{I}_1(k) + \frac{1}{\delta_c} \frac{\partial \mathcal{I}_1(k)}{\partial \ln \sigma_M}, \quad (103)$$

$$Q_2(k) = b_2^L \mathcal{I}_2(k) + \frac{1 + \delta_c b_1^L}{\delta_c^2} \frac{\partial \mathcal{I}_2(k)}{\partial \ln \sigma_M}. \quad (104)$$

D. Effects of Mass Selection

The above calculations assume that all halos have the same mass, M . In reality, halos of different masses are contained in a given sample. When the finiteness of mass range is not negligible, the global and local number densities of halos are given by

$$N(M) = \int dM \phi(M) n(M), \quad (105)$$

$$N(\mathbf{x}, M) = \int dM \phi(M) n(\mathbf{x}, M), \quad (106)$$

respectively, where $\phi(M)$ is an arbitrary selection function of mass. When the mass of halos in a range $M_1 < M < M_2$ are evenly selected, the selection function is given by $\phi(M) = 1$ when $M_1 < M < M_2$ and $\phi(M) = 0$ otherwise. When the mass range is negligibly small, $\phi(M') = \delta_D(M' - M)$.

The number density contrast in Lagrangian space is given by $\delta_h^L(\mathbf{x}) = N(\mathbf{x}, M)/N(M) - 1$. Following a similar procedure to obtain Eq. (82), we have

$$c_n^L(\mathbf{k}_1, \dots, \mathbf{k}_n) = \frac{(-1)^n \int dM \frac{\phi(M)}{M} \frac{\partial}{\partial M} \left[\frac{\partial^n P(M, \delta_c)}{\partial \delta_c^n} W(k_1 R) \dots W(k_n R) \right]}{\int dM \frac{\phi(M)}{M} \frac{\partial P(M, \delta_c)}{\partial M}}. \quad (107)$$

instead of Eq. (82). Taking account of Eqs. (78) and (82), we find

$$c_n^L(\mathbf{k}_1, \dots, \mathbf{k}_n) = \frac{\int dM \phi(M) n(M) c_n^L(\mathbf{k}_1, \dots, \mathbf{k}_n; M)}{\int dM \phi(M) n(M)}, \quad (108)$$

where $c_n^L(\mathbf{k}_1, \dots, \mathbf{k}_n; M)$ is the renormalized bias function for a fixed mass M derived in the previous subsection, Eqs. (88), (91) or (92). Quite naturally, Eq. (108) shows that the renormalized bias functions for mass-selected halo samples are obtained by averaging over mass-dependent bias functions weighted by selected number of halos.

E. Cancellation of highest-order bias parameters in Press-Schechter mass function

In the case of PS mass function, there is a remarkable property that the n th-order renormalized bias function c_n^L only depend on next two lower-order bias parameters b_{n-1}^L and b_{n-2}^L , as shown below.

The scale-independent parameter b_n^L of Eq. (71) in the case of PS mass function is given by

$$b_n^L(M) = \frac{\nu^{n-1} H_{n+1}(\nu)}{\delta_c^n}, \quad (109)$$

where $H_n(\nu) = e^{\nu^2/2} (-d/d\nu)^n e^{-\nu^2/2}$ denotes Hermite polynomials. Using a recursion relation of the Hermite polynomials, $H_{n+1}(\nu) = \nu H_n(\nu) - n H_{n-1}(\nu)$, we observe that remarkable cancellations in the series of Eq. (93) occur and just a single term survives as

$$A_n(M) = \nu^n H_n(\nu) = \frac{\delta_c^{n+1}}{\sigma_M^2} b_{n-1}^L(M), \quad (110)$$

where $b_{-1}^L(M) \equiv \sigma_M^2/\delta_c$ for consistency. For $n = 1, 2$, we have

$$A_1(M) = \nu^2, \quad A_2(M) = \nu^2 \delta_c b_1^L(M). \quad (111)$$

Interestingly, the highest-order parameter b_n^L vanishes in A_n , and it is simply proportional to the next lower-order parameter b_{n-1}^L in this case of PS mass function. Accordingly, the renormalized bias function c_n^L of n th order depends only on lower-order bias parameters b_{n-1}^L and b_{n-2}^L in the form of Eq. (91) with Eq. (110). In the next subsection, this notable property turns out to be the reason why the scale-dependent bias from the primordial bispectrum is roughly proportional to the first-order bias parameter b_1^L instead of the second-order parameter b_2^L .

However, the exact cancellations do not occur in other cases than the PS mass function. For example, in the case of ST mass function with the bias parameters of Eqs. (73) and (74), coefficients of the renormalized bias functions, Eqs. (96) and (97) reduce to

$$A_1(M) = q\nu^2 + \frac{2p}{1 + (q\nu^2)^p}, \quad (112)$$

$$A_2(M) = q\nu^2 \delta_c b_1^L(M) + \frac{2p(q\nu^2 + 2p + 1)}{1 + (q\nu^2)^p}, \quad (113)$$

and so forth. The leading term of A_n is still proportional to the next lower-order bias parameter b_{n-1}^L , but correction terms, which are proportional to p , additionally appear. In the case

of PS mass function, $p = 0$ and $q = 1$, the above equations agree with Eq. (110) of $n = 1, 2$ as they should. Similarly, in the case of MICE mass function with the bias parameters of Eqs. (75) and (76), we have

$$A_1(M) = \frac{2c}{\sigma^2} + 1 - \frac{a}{1 + b\sigma^a}, \quad (114)$$

$$A_2(M) = \frac{2c}{\sigma^2} \delta_c b_1^L(M) + \frac{2c}{\sigma^2} + 2 - \frac{a(2c/\sigma^2 - a + 3)}{1 + b\sigma^a}, \quad (115)$$

and so forth. Again, when we substitute $a = 1$, $b = 0$ and $c = \delta_c^2/2$, the above equations agree with Eq. (110) of $n = 1, 2$.

F. Relation to the previous formula derived by the peak-background split

We explicitly show below that predictions of the peak-background split are re-derived as a special case of the general formula we have derived. First we drop the terms Q_0 , Q_1 in Eq. (25), which are subdominant on large scales, and only consider the dominant term $Q_2(k)$. In this approximation, the scale-dependent bias is approximately given by $\Delta b(k) \approx Q_2(k)/2P_L(k)$, i.e.,

$$\Delta b(k) \approx \frac{1}{2P_L(k)} \int \frac{d^3k'}{(2\pi)^3} c_2^L(\mathbf{k}', \mathbf{k} - \mathbf{k}') B_L(k, k', |\mathbf{k} - \mathbf{k}'|). \quad (116)$$

Substituting the second-order renormalized bias function c_2^L in the form of Eq. (91) with $n = 2$ into the above equation, we have

$$\Delta b(k) \approx \frac{\sigma_M^2}{2\delta_c^2} \left[A_2 I(k) + A_1 \frac{\partial I(k)}{\partial \ln \sigma_M} \right], \quad (117)$$

where

$$\begin{aligned} I(k) &\equiv \frac{I_2(k)}{\sigma_M^2 P_L(k)} \\ &\approx \frac{1}{\sigma_M^2 P_L(k)} \int \frac{d^3k'}{(2\pi)^3} W^2(k'R) B_L(k, k', |\mathbf{k} - \mathbf{k}'|). \end{aligned} \quad (118)$$

When bias parameters of the PS mass function are used, the parameter A_1 , A_2 are given by Eq. (111), and Eq. (117) reduces to

$$\Delta b(k) \approx \frac{1}{2} \delta_c b_1^L I(k) + \frac{1}{2} \frac{\partial I(k)}{\partial \ln \sigma_M}. \quad (119)$$

This equation is exactly the same as a recent prediction of the peak-background split [16, 17]. In the literature, the window function $W(kR)$ is sometimes additionally divided into the function $I(k)$ because the bias is defined with respect to the smoothed density field in the latter case (private communications with V. Desjacques). Earlier predictions in the literature [5, 7, 15] are reproduced from the first term of Eq. (119). Although the second term is subdominant in the high-peak limit, it is significant for most relevant peak heights [16, 17]. In the local model of non-Gaussianity, the second term vanishes on sufficiently large scales.

Importantly, our derivation does not use the approximation of the peak-background split to obtain the same prediction. Therefore, the known result of Eq. (119) turns out not to particularly depend on the approximation of the peak-background split. However, we have found that this equation is consistent only with the PS mass function. That is not surprising, because the arguments of peak-background split use an auxiliary Gaussian field as a fundamental field in the analysis. The original PS mass function is properly derived by assuming the Gaussian statistics for the linear density field. Applying the Gaussian statistics to the auxiliary field is only consistent with the original PS mass function in the peak-background split.

Our derivation, on the other hand, does not use any auxiliary Gaussian field, and therefore gives natural extensions to the formula with general mass functions as we have seen. Even when subdominant terms on large scales, Q_0 and Q_1 , are neglected, our result predicts that the known result of Eq. (119) should be modified to Eq. (117) with Eqs. (96) and (97), i.e.,

$$\Delta b(k) \approx \frac{\sigma_M^2}{2\delta_c^2} \left[(2 + 2\delta_c b_1^L + \delta_c^2 b_2^L) I(k) + (1 + \delta_c b_1^L) \frac{dI(k)}{d \ln \sigma_M} \right]. \quad (120)$$

Taking the ST mass function for example, the above equation reduces to

$$\Delta b(k) \approx \left[\frac{q\delta_c b_1^L}{2} + \frac{1}{v^2} \frac{p(qv^2 + 2p + 1)}{1 + (qv^2)^p} \right] I(k) + \left[\frac{q}{2} + \frac{1}{v^2} \frac{p}{1 + (qv^2)^p} \right] \frac{dI(k)}{d \ln \sigma_M}. \quad (121)$$

This equation is still a new result in the literature, even though other correction terms, Q_0 and Q_1 , are neglected. The previously known result, Eq. (119), is obtained only when the PS mass function is assumed, $p = 0$, $q = 1$. Taking the MICE mass function, the coefficients of Eq. (121) are replaced by Eqs. (114) and (115) instead of Eqs. (112) and (113).

One should note that although the ST (MICE) mass function is derived from Gaussian simulations, contributions of the primordial non-Gaussianity to the mass function are higher orders in Eq. (121), and can be neglected in the lowest-order approximation of this paper. Although higher-order corrections are beyond the scope of this paper, they could be relevant in the quantitative analysis of actual data.

In the specific models of primordial non-Gaussianity, large-scale limits of the function $I(k)$ with asymptotic bispectra of

Eqs. (47)–(50) are given by

$$I^{\text{loc.}}(k) \approx \frac{4f_{\text{NL}}}{\mathcal{M}(k)}, \quad (122)$$

$$I^{\text{eq.}}(k) \approx \frac{12f_{\text{NL}}}{\mathcal{M}(k)} k^2 \left[k^{2\alpha_s} \gamma_{2+2\alpha_s} - \frac{(1 + \alpha_s)^2}{3} \gamma_2 \right], \quad (123)$$

$$I^{\text{fol.}}(k) \approx \frac{6f_{\text{NL}}}{\mathcal{M}(k)} k \gamma_1, \quad (124)$$

$$I^{\text{ort.}}(k) \approx -\frac{12f_{\text{NL}}}{\mathcal{M}(k)} k \gamma_1, \quad (125)$$

where

$$\gamma_\alpha(M) = \frac{1}{\sigma_M^2} \int \frac{d^3k}{(2\pi)^3} k^{-\alpha} W^2(kR) P_L(k). \quad (126)$$

Predictions of the scale-dependent bias in these specific models are made when the above equations are substituted in Eq. (121). In the scale-free power spectrum, $n_s = 1$ ($\alpha_s = 0$), Eq. (123) is simply given by

$$I^{\text{eq.}}(k) \approx \frac{8f_{\text{NL}}}{\mathcal{M}(k)} k^2 \gamma_2, \quad (n_s = 1). \quad (127)$$

For highly biased objects, $A_2 \approx qv^2 \delta_c b_1^L \gg A_1$, the dominant term of Eq. (121) is given by

$$\Delta b(k) \approx \frac{q\delta_c b_1^L}{2} I(k), \quad (128)$$

which agrees with previous predictions [5, 6, 15] in the case of PS mass function, $q = 1$. In the case of ST mass function, we find the factor $q \approx 0.707$ should additionally be present. Since the ST mass function gives better fit to the halo mass function in numerical simulations, our result suggests that these previous predictions overestimate the amplitude of scale-dependent bias in the high-peak limit. In the case of MICE mass function, the coefficient q in Eq. (128) is replaced by $2c/\delta_c^2 = 0.729(1+z)^{-0.024}$.

In fact, recent numerical simulations actually prefer that the previous theoretical predictions overestimate the amplitude of scale-dependent bias [23–27]. When the parameter q in Eq. (128) is freely fit to numerical simulations, they found $q = 0.6 - 1$ although the value varies from simulation to simulation, depending on the algorithm to identify the halos, etc. However, it is encouraging that the value is not so different from $q = 0.707$. It is also natural that numerical simulations do not fit well to the high-peak formula of Eq. (128), because the correction terms in Eq. (121) are not negligible for relevant ranges of halo mass. More quantitative comparisons of the newly derived Eq. (120) with numerical simulations, together with estimating higher-order corrections and improving nonlocal bias models, are left for future work.

V. NUMERICAL COMPARISONS

In this subsection, we numerically evaluate the analytical results derived above, and compare them with other approximate methods. For this purpose, we use the halo bias as a specific example, where the bias functions are given by Eqs. (98)

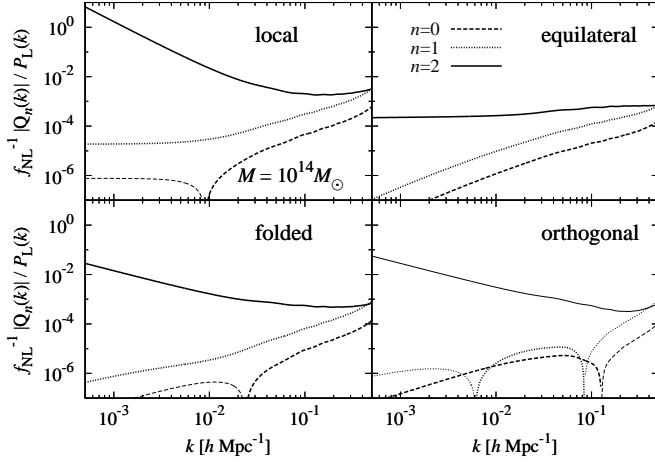


FIG. 5: The functions $Q_n(k)$ divided by $f_{\text{NL}} P_L(k)$ (dashed: $n = 0$, dotted: $n = 1$, solid: $n = 2$) at redshift $z = 1$. Negative values are shown in thin lines. The halo model with mass $M = 10^{14} M_\odot$ is assumed in calculating $Q_1(k)$ and $Q_2(k)$. Different panels correspond to different models of primordial non-Gaussianity as indicated.

and (99) up to second order. We assume the halo sample has a redshift of $z = 1$, as a typical example.

For numerical integrations, it is useful to rewrite the function Q_0 of Eqs. (17) and (18), and the functions $I_1(k)$ and $I_2(k)$ of Eqs. (100)–(102) into the following two-dimensional integrals:

$$Q_0(k) = \frac{k^3}{4\pi^2} \int_0^\infty dr \int_{-1}^1 dx \left[2rx - \frac{4}{7} \frac{r^2(1-x^2)}{1+r^2-2rx} \right] \times B_L(k, kr, k\sqrt{1+r^2-2rx}), \quad (129)$$

$$I_1(k) = \frac{k^3}{2\pi^2} \int_0^\infty dr \int_{-1}^1 dx rx W(kR\sqrt{1+r^2-2rx}) \times B_L(k, kr, k\sqrt{1+r^2-2rx}), \quad (130)$$

$$I_2(k) = \frac{k^3}{4\pi^2} \int_0^\infty dr \int_{-1}^1 dx r^2 W(krR) W(kR\sqrt{1+r^2-2rx}) \times B_L(k, kr, k\sqrt{1+r^2-2rx}). \quad (131)$$

In terms of the functions $I_1(k)$ and $I_2(k)$, the functions $Q_1(k)$ and $Q_2(k)$ are given by Eqs. (103) and (104). In numerically calculating the derivatives $\partial I_n / \partial \ln \sigma_M$, it is useful to note that the derivative of the top-hat window function [Eq. (63)] is given by

$$\frac{dW(x)}{dx} = -\frac{3j_2(x)}{x} = \frac{3(x^2 - 3)\sin x + 9x \cos x}{x^4}, \quad (132)$$

where $j_2(x)$ is the second-order spherical Bessel function.

In Fig. 5, the functions $Q_n(k)$ ($n = 0, 1, 2$) are plotted in the case of $z = 1$ and $M = 10^{14} M_\odot$. We assume four models of primordial non-Gaussianity, Eqs. (38)–(41), and bias functions with ST mass function, Eqs. (73), (74), (98) and (99). As we have seen in Sec. III B, the function $Q_2(k)$ is dominant over $Q_0(k)$ and $Q_1(k)$ on sufficiently large scales. In Fig. 6,

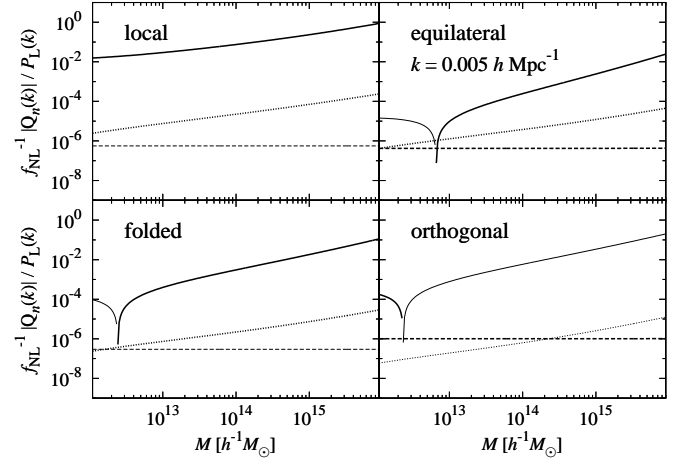


FIG. 6: The functions $Q_n(k)$ divided by $f_{\text{NL}} P_L(k)$ with a fixed scale $k = 0.005 h \text{ Mpc}^{-1}$ at redshift $z = 1$, plotted against the halo mass (dashed: $n = 0$, dotted: $n = 1$, solid: $n = 2$). Negative values are shown in thin lines. Different panels correspond to different models of primordial non-Gaussianity as indicated.

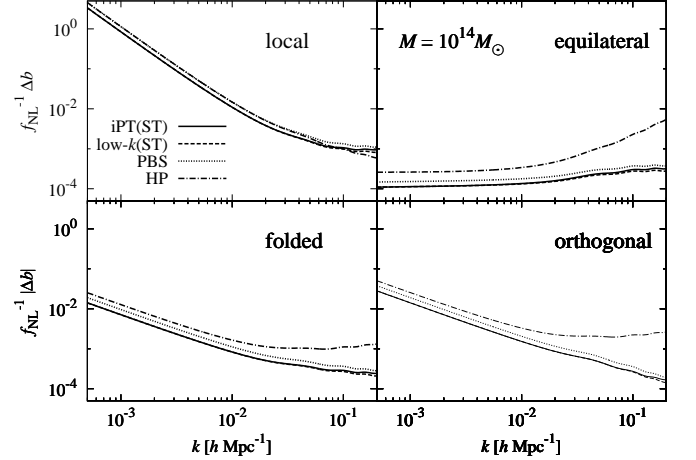


FIG. 7: Scale-dependent bias $\Delta b(k)$ divided by f_{NL} for halos of mass $M = 10^{14} M_\odot$. Solid lines correspond to predictions of iPT with ST mass function. Other lines correspond to predictions of the peak-background split (PBS, dotted lines), the low- k limit of iPT with ST mass function (dashed lines), and the high-peak limit of PBS (dot-dashed lines). Positive and negative values are represented by thick and thin lines, respectively. When we use the PS mass function for the iPT, low- k limit of iPT and PBS gives the same results.

the same functions are plotted against the halo mass with a fixed scale $k = 0.005 h \text{ Mpc}^{-1}$. On large scales, the function $Q_2(k)$ is dominant as expected, and the scale-dependent bias is approximately given by Eq. (42).

In Fig. 7, the scale-dependent bias $\Delta b(k)$ divided by f_{NL} is plotted for $M = 10^{14} M_\odot$ with four models of primordial non-Gaussianity. In solid lines, the predictions of iPT with ST mass function [Eqs. (25), (98), (99), (73) and (74)] are plotted. The predictions of the peak-background split (PBS) [Eq. (119)] are plotted in dotted lines. In dashed lines, the

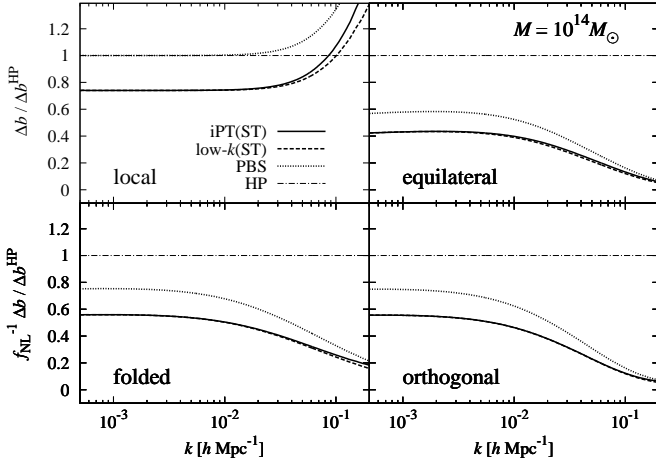


FIG. 8: The same as Fig. 7, but the scale-dependent bias $\Delta b(k)$ is normalized by the large-scale, high-peak approximation $\Delta b^{\text{HP}}(k)$.

predictions of the large-scale (low- k) limit of iPT with ST mass function [Eq. (121)] are plotted. In dot-dashed lines, predictions of the PBS with high-peak and large-scale limits are plotted. The last predictions are given by

$$\Delta b^{\text{HP}}(k) = \frac{f_{\text{NL}} \delta_c b_1^{\text{L}}}{M(k)} \times \begin{cases} 2, & (\text{local}), \\ 4k^2 \gamma_2 & (\text{equilateral}), \\ 3k \gamma_1 & (\text{folded}), \\ -6k \gamma_1 & (\text{orthogonal}), \end{cases} \quad (133)$$

which are derived from Eqs. (122), (127), (124), (125), and the first term of Eq. (119). For the equilateral model, we use the approximation $n_s = 1$ for simplicity, and adopt Eq. (127) instead of Eq. (123). The first case of Eq. (133) is exactly the same as the original formula for the local model derived in Refs. [5, 9]. The third and fourth cases exactly match the results of Ref. [15] for the folded and orthogonal models. For the equilateral model, however, the prefactor 4 is replaced by 6 in Ref. [15], because angular-dependences of the bispectrum are neglected in the latter. The factor 4 is more accurate as shown below. In Fig. 8, relative amplitudes with respect to $\Delta b^{\text{HP}}(k)$ of Eq. (133) are plotted.

As expected, the low- k limit of iPT (using only Q_2) is an extremely good approximation on large scales ($k \lesssim 0.05 h/\text{Mpc}$). The large-scale asymptotes of iPT with ST mass function is smaller than those of peak-background split. These differences originate from the different mass functions. If we adopt PS mass function in iPT, the asymptotes of iPT and PBS exactly agree.

The simple predictions of $\Delta b^{\text{HP}}(k)$ have correct slopes in large-scale limits. The amplitudes are not so accurate for non-local-type non-Gaussianities, even if we assume PS mass function instead of ST mass function. On smaller scales ($k \gtrsim 0.01 h/\text{Mpc}$), the slopes of $\Delta b^{\text{HP}}(k)$ are not accurate enough. The deviations from the peak-background split in $k \gtrsim 0.01 h^{-1} \text{Mpc}$ are also pointed out in earlier work in the high-peak limit of thresholded regions [6, 56]. However, higher-order loop corrections which we do not consider in this

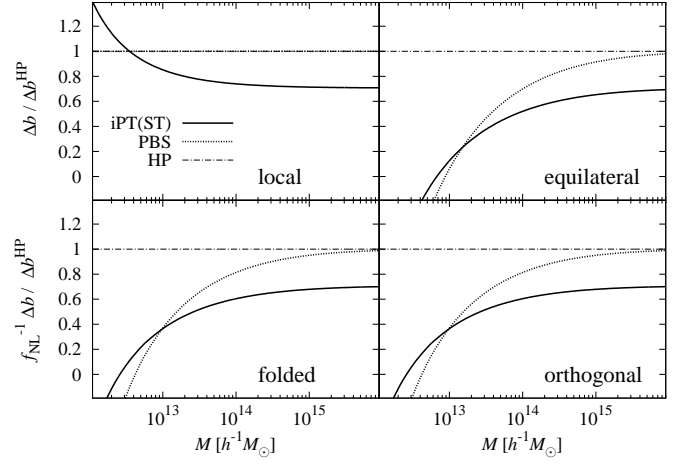


FIG. 9: The normalized scale-dependent bias in large-scale limits ($k \rightarrow 0$, however, we numerically adopt $k = 10^{-4} h/\text{Mpc}$ to plot this figure). As in Fig. 8, the values are normalized by the simple approximation $\Delta b^{\text{HP}}(k)$. Meanings of different types of lines are the same as in Figs. 7 and 8.

paper might affect the behaviors of scale-dependent bias on scales of $k \gtrsim 0.05 h^{-1} \text{Mpc}$.

In Fig. 9, the normalized scale-dependent bias against the halo mass is plotted in the large-scale limits ($k \rightarrow 0$). The purpose of this figure is to illustrate the mass dependence of the plateaux on large scales in Fig. 8. The predictions of peak-background split and high-peak limit are asymptotically agree with each other for high-mass halos, as they should. In large-mass limits, the predictions of peak-background split and iPT are different by a factor of $q \approx 0.7$, which is explained by Eq. (128).

VI. SCALE-DEPENDENT BIAS IN REDSHIFT SPACE

Generalizing the results obtained so far in real space to those in redshift space is fairly straightforward in the framework of iPT. The redshift-space distortions of scale-dependent bias in the presence of local-type non-Gaussianity have been investigated in the literature [57–59], relying on the high-peak limit or the peak-background split. With the iPT, it is straightforward to generalize those results without restricting to the local-type non-Gaussianity, and we do not need to rely on the high-peak limit or the peak-background split.

When the weak time dependences in the perturbation kernels are neglected, the n th order perturbations are approximately proportional to D^n , and the redshift-space counterpart of the kernel L_n is given by [36]

$$L_n^s = R^{(n)} L_n, \quad (134)$$

where $R^{(n)}$ is a 3×3 matrix with elements

$$R_{ij}^{(n)} = \delta_{ij} + n f \hat{z}_i \hat{z}_j, \quad (135)$$

where $f = d \ln D / d \ln a = \dot{D} / H D$ is the linear growth rate, and \hat{z}_i is the i th element of the unit vector $\hat{\mathbf{z}}$ along the line of

sight. The perturbation kernels L_n in the multipoint propagators of Eqs. (5) and (6) are replaced by L_n^s in redshift space. Specifically we have

$$\mathbf{k} \cdot \mathbf{L}_n^s = (\mathbf{k} + n f \mu k \hat{\mathbf{z}}) \cdot \mathbf{L}_n, \quad (136)$$

where $\mu = \mathbf{k} \cdot \hat{\mathbf{z}}/k$ is the direction cosine of the wavevector \mathbf{k} with respect to the line of sight.

Substituting the resulting multipoint propagators in redshift space into Eq. (13), we have an expression for the non-Gaussian part of the power spectrum in redshift space. In evaluating the expression, the following integrals are useful:

$$\int \frac{d^3 k'}{(2\pi)^3} L_2(\mathbf{k}', \mathbf{k} - \mathbf{k}') B_L(k, k', |\mathbf{k} - \mathbf{k}'|) = \frac{3}{7} \frac{\mathbf{k}}{k^2} R_2(k), \quad (137)$$

$$\begin{aligned} \int \frac{d^3 k'}{(2\pi)^3} L_{1i}(\mathbf{k}') L_{1j}(\mathbf{k} - \mathbf{k}') B_L(k, k', |\mathbf{k} - \mathbf{k}'|) \\ = \frac{k_i k_j}{k^4} \left[2R_1(k) - \frac{1}{2} R_2(k) \right] - \frac{\delta_{ij}}{2k^2} R_2(k), \end{aligned} \quad (138)$$

$$\int \frac{d^3 k'}{(2\pi)^3} c_1^L(\mathbf{k}') L_1(\mathbf{k} - \mathbf{k}') B_L(k, k', |\mathbf{k} - \mathbf{k}'|) = \frac{1}{2} \frac{\mathbf{k}}{k^2} Q_1(k), \quad (139)$$

$$\int \frac{d^3 k'}{(2\pi)^3} c_2^L(\mathbf{k}', \mathbf{k} - \mathbf{k}') B_L(k, k', |\mathbf{k} - \mathbf{k}'|) = Q_2(k), \quad (140)$$

where the functions $Q_1(k)$ and $Q_2(k)$ are defined by Eqs. (17), (18), (19), and the functions $R_1(k)$ and $R_2(k)$ are defined by

$$R_n(k) = \int \frac{d^3 k'}{(2\pi)^3} \hat{R}_n(\mathbf{k}, \mathbf{k}') B_L(k, k', |\mathbf{k} - \mathbf{k}'|), \quad (141)$$

where

$$\hat{R}_1 = \frac{\mathbf{k} \cdot \mathbf{k}'}{k'^2}, \quad (142)$$

$$\hat{R}_2 = \frac{k^2 k'^2 - (\mathbf{k} \cdot \mathbf{k}')^2}{k'^2 |\mathbf{k} - \mathbf{k}'|^2}. \quad (143)$$

Eqs. (137)–(140) are derived by noting that integrals on the left-hand sides are functions of only \mathbf{k} , and using the rotational covariance (similar technique is used in Ref. [36]). The function $Q_0(k)$ is related by

$$Q_0(k) = 2R_1(k) - \frac{4}{7} R_2(k). \quad (144)$$

The functions $R_1(k)$ and $R_2(k)$ reduce to two-dimensional integrals as

$$R_1(k) = \frac{k^3}{4\pi^2} \int_0^\infty dr \int_{-1}^1 dx r x B_L(k, kr, k \sqrt{1+r^2-2rx}), \quad (145)$$

$$\begin{aligned} R_2(k) = \frac{k^3}{4\pi^2} \int_0^\infty dr \int_{-1}^1 dx \frac{r^2(1-x^2)}{1+r^2-2rx} \\ \times B_L(k, kr, k \sqrt{1+r^2-2rx}). \end{aligned} \quad (146)$$

Eventually, the non-Gaussian part of the power spectrum in redshift space is given by

$$\begin{aligned} \Delta P_X^s(k, \mu) = [b_1(k) + f\mu^2] \left\{ 2(1 + f\mu^2)^2 R_1(k) \right. \\ \left. - \left[\frac{4}{7}(1 + 2f\mu^2) + \frac{1}{2} f^2 \mu^2 (\mu^2 + 1) \right] R_2(k) \right. \\ \left. + (1 + f\mu^2) Q_1(k) + Q_2(k) \right\}. \end{aligned} \quad (147)$$

When we put $f = 0$ in the above equation, the power spectrum in real space, Eq. (15), is recovered. In the large-scale limit $k \rightarrow 0$, we have $R_1(k), R_2(k), Q_1(k) \ll Q_2(k)$, and the asymptotic form of the power spectrum is given by

$$\Delta P_X(k, \mu) \approx [b_1(k) + f\mu^2] Q_2(k). \quad (148)$$

The angular dependence of the power spectrum is conveniently decomposed into multipoles as

$$\Delta P_X^s(k, \mu) = \sum_{l=0}^{\infty} \Delta p_l(k) P_l(\mu), \quad (149)$$

where $P_l(\mu)$ are the Legendre polynomials, and $\Delta p_l(k)$ are the multipole moments. Using the orthogonal relations of the Legendre polynomials, we have

$$\Delta p_l(k) = \frac{2l+1}{2} \int_{-1}^1 d\mu P_l(\mu) \Delta P_X^s(k, \mu). \quad (150)$$

The monopole component $\Delta p_0(k)$ corresponds to the angular average of the power spectrum in redshift space, and higher-order moments characterize anisotropies in the power spectrum, relative to the line of sight. We decompose each multipole moment as $p_l(k) = p_l^G(k) + \Delta p_l(k)$, where $p_l^G(k)$ is the multipole moment of the Gaussian part of the power spectrum $P_X^G(k, \mu)$.

The multipole decomposition of the linear power spectrum in redshift space $P^G(k, \mu) = [b_1(k) + f\mu^2]^2 P_L(k)$ is well known [60, 61]:

$$p_0^G(k) = \left\{ [b_1(k)]^2 + \frac{2}{3} b_1(k) f + \frac{1}{5} f^2 \right\} P_L(k), \quad (151)$$

$$p_2^G(k) = \left\{ \frac{4}{3} b_1(k) f + \frac{4}{7} f^2 \right\} P_L(k), \quad (152)$$

$$p_4^G(k) = \frac{8}{35} f^2 P_L(k). \quad (153)$$

For the multipole decomposition of the non-Gaussian part,

Eq. (150), we have

$$\begin{aligned} \Delta p_0(k) = & 2 \left[\frac{f}{3} + \frac{2f^2}{5} + \frac{f^3}{7} + \left(1 + \frac{2f}{3} + \frac{f^2}{5} \right) b_1(k) \right] R_1(k) \\ & - 2 \left[\frac{2f}{21} + \frac{4f^2}{35} + \frac{3f^3}{35} + \left(\frac{2}{7} + \frac{4f}{21} + \frac{2f^2}{15} \right) b_1(k) \right] R_2(k) \\ & + \left[\frac{f}{3} + \frac{f^2}{5} + \left(1 + \frac{f}{3} \right) b_1(k) \right] Q_1(k) \\ & + \left[\frac{f}{3} + b_1(k) \right] Q_2(k), \end{aligned} \quad (154)$$

$$\begin{aligned} \Delta p_2(k) = & 4f \left[\frac{1}{3} + \frac{4f}{7} + \frac{5f^2}{21} + \left(\frac{2}{3} + \frac{2f}{7} \right) b_1(k) \right] R_1(k) \\ & - f \left[\frac{8}{21} + \frac{32f}{49} + \frac{11f^2}{21} + \left(\frac{16}{21} + \frac{13f}{21} \right) b_1(k) \right] R_2(k) \\ & + 2f \left[\frac{1}{3} + \frac{2f}{7} + \frac{1}{3} b_1(k) \right] Q_1(k) + \frac{2f}{3} Q_2(k), \end{aligned} \quad (155)$$

$$\begin{aligned} \Delta p_4(k) = & 16f^2 \left[\frac{2}{35} + \frac{3f}{77} + \frac{1}{35} b_1(k) \right] R_1(k) \\ & - \frac{4f^2}{35} \left[\frac{16}{7} + \frac{26f}{11} + b_1(k) \right] R_2(k) + \frac{8f^2}{35} Q_1(k), \end{aligned} \quad (156)$$

$$\Delta p_6(k) = \frac{32f^3}{231} R_1(k) - \frac{8f^3}{231} R_2(k). \quad (157)$$

Although the above expressions are messy, most of the terms are negligibly small in the large-scale limit $k \rightarrow 0$, and only terms proportional to $Q_2(k)$ are dominant, i.e.,

$$\Delta p_0(k) \approx \left(\frac{f}{3} + b_1 \right) Q_2(k), \quad \Delta p_2(k) \approx \frac{2f}{3} Q_2(k), \quad (158)$$

$$\Delta p_4(k), \Delta p_6(k) \ll \Delta p_0(k), \Delta p_2(k), \quad (159)$$

where the linear (Gaussian) bias parameter b_1 is generally scale-independent in the large-scale limit. The factor $f/3 + b_1$ in the monopole component is previously derived in a special case of the local-type non-Gaussianity with the high-peak limit [59].

When the bias is large enough, $c_2^L \gg c_1^L \gg 1$, and $Q_2 \gg Q_1 \gg R_1, R_2$, we have

$$p_0^G(k) \approx [b_1(k)]^2 P_L(k) \gg p_2^G(k) \gg p_4^G(k), \quad (160)$$

$$\Delta p_0(k) \approx b_1(k) Q_2(k) \gg \Delta p_2(k) \gg \Delta p_4(k) \gg \Delta p_6(k). \quad (161)$$

The above equations show that the redshift-space clustering reduces to the real-space clustering when the bias is large enough. This fact is naturally expected because the peculiar velocities of high peaks or high-mass halos are sufficiently small.

In Fig. 10, relative differences of the lower-order multipoles, $\Delta p_l(k)/p_0^G(k)$, are plotted for $M = 10^{14} M_\odot$. We only plot the lowest two multipoles $l = 0, 2$, since the higher-order multipoles $l = 4, 6$ are small enough. The scale dependences of multipoles with $l = 0, 2$ have a similar slope on large scales but different amplitudes. These properties are explained by the dominant contributions on large scales, Eq. (158). The ratio of those two multipoles, in the large-scale limit, is given

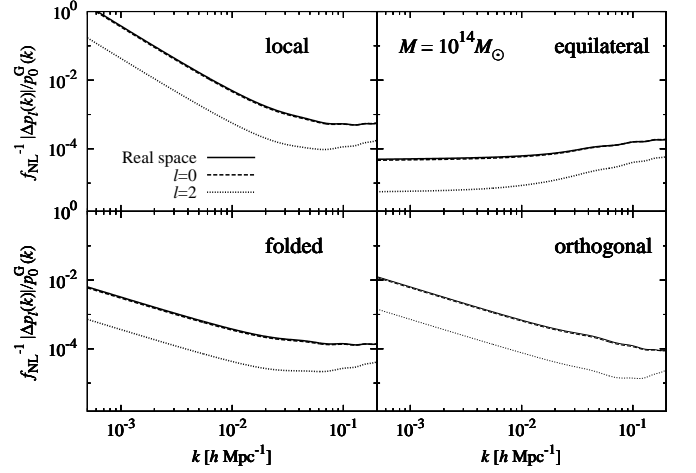


FIG. 10: Relative differences of the multipoles in the halo power spectrum $\Delta p_l(k)/p_l^G(k)$ with $M = 10^{14} M_\odot$ (dashed lines: $l = 0$, dotted lines: $l = 2$). Solid lines corresponds to the relative differences of the real-space power spectrum, which are the same as the solid lines in Fig. 7. Positive and negative values are represented by thick and thin lines, respectively.

by

$$\frac{\Delta p_2(k)}{\Delta p_0(k)} \approx \frac{2f}{f + 3b_1} = \frac{2}{1 + 3/\beta}, \quad (162)$$

where $\beta \equiv f/b_1$ is the linear redshift-space distortion parameter. This ratio is small for highly biased objects, or massive halos.

Relative monopole components $\Delta p_0(k)/p_0^G(k)$ on large scales are not so different between real space and redshift-space. This property is true even in the low-mass halos. Therefore, the scale-dependent bias is not so affected by the redshift-space distortions when only the monopole component is concerned. However, the quadrupole component may be used in constraining the primordial non-Gaussianity.

In Fig. 11, relative differences of the lower-order multipoles are plotted against the mass of halo, where the scale is fixed to $k = 0.005 h^{-1} \text{Mpc}$. As described above, the relative monopole components are similar in real and redshift spaces, irrespective to the mass of halos. They are asymptotically the same in the high-mass limit, because of Eqs. (160) and (161). In the same limit, the ratio $\Delta p_2/\Delta p_0$ approaches to $2\beta/3$ according to Eq. (162).

VII. CONCLUSIONS

The iPT is a general framework of the perturbation theory in the presence of bias. In this paper, we first apply this framework to deriving the relation between the scale-dependent bias and the primordial non-Gaussianity. Approximations such as the peak-background split and the high-peak limit, which are usually adopted in the literature to estimate the scale-dependent bias, are not required. The redshift-space distortions of the scale-dependent bias are also evaluated. Thus, in

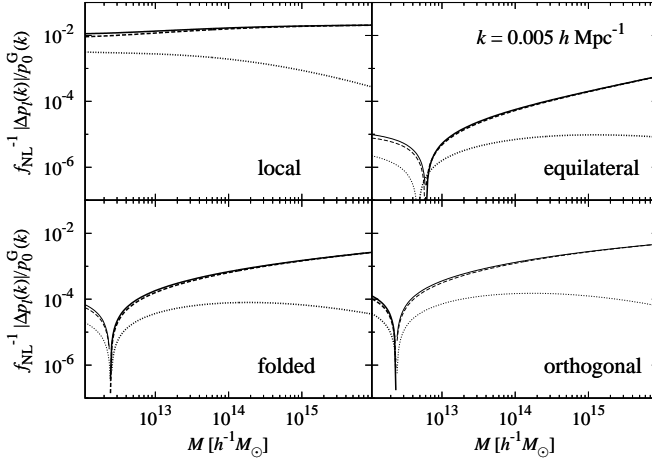


FIG. 11: Relative differences of the multipoles in the halo power spectrum as a function of the halo mass for a fixed scale $k = 0.005 h^{-1} \text{Mpc}^{-1}$. Meanings of different types of lines are the same as in Fig. 10 (solid lines: real space, dashed lines: $l = 0$, dotted lines: $l = 2$).

this paper, we have derived the most general formula so far of the scale-dependent bias with primordial non-Gaussianity in the literature.

For the scale-dependent bias in real space, the most fundamental equation in this paper is provided by Eq. (25), where $Q_n(k)$ is linearly dependent on the primordial bispectrum. We find that the slope of the scale-dependent bias in the large-scale limit is determined only by primordial bispectra in the squeezed limit, and is independent on detailed models of bias. This property explains the fact that different models of bias have predicted the same slope of the scale-dependent bias in the literature.

We derive the shape of renormalized bias functions, generalizing the concept of simple Press-Schechter approach. The general expression of renormalized bias functions in this approach is given by Eq. (82). In the case of universal mass function, the renormalized bias functions are given by Eq. (91), or equivalently Eq. (92). The previously known results in the approximation of peak-background split are reproduced when the PS mass function is assumed in our results [Eq. (119)]. When the mass function deviates from the PS form, our results suggest that the form of scale-dependent bias should be corrected. The general formula of scale-dependent bias on large scales is given by Eq. (120). This equation is one of the main outcomes in this paper. Most of the previous results regarding

the scale-dependent bias from the primordial non-Gaussianity are derived as special cases of this equation.

The evaluations of the redshift-space distortions in the scale-dependent bias are straightforward in the framework of iPT. The result is given by Eq. (147), or in terms of multipole coefficients, Eqs. (154)–(157). On large scales, however, dominant terms in these equations are simply given by Eqs. (158) and (159). When the bias is large enough, the redshift-space distortions do not affect the scale-dependence of bias much [Eqs. (160) and (161)]. Even when the bias is not large enough, the redshift-space distortions have little effects at least in the non-Gaussian models we have considered (Figs. 10 and 11).

While highly biased objects have large amplitudes of power spectrum, the number of objects is small and the shot noise is large. Thus highly biased objects are not suitable for testing the primordial non-Gaussianity. On the other hand, the amplitude of power spectrum is small for less biased objects, and the clustering signals are small. Consequently, there should be an optimal objects with sufficiently large bias and sufficiently large numbers at the same time for realistically constraining the primordial non-Gaussianity by galaxy surveys. The high-peak limit or the peak-background split are not necessarily valid in some cases. The results of this paper provide the most accurate formula of the scale-dependent bias in the literature. They should be useful in theoretical investigations as well as in constraining the primordial non-Gaussianity with realistic galaxy surveys. Applications of the results in this paper, including the Fisher analysis of the future galaxy surveys, higher-order analyses of primordial non-Gaussianity, are now in progress. For more accurate modeling of the scale-dependent bias, it should be necessary to improve the nonlocal bias model beyond the simple halo approach. Investigations in this direction will be addressed in future work.

Acknowledgments

I wish to thank S. Yokoyama and V. Desjacques for helpful discussion. I acknowledge support from the Ministry of Education, Culture, Sports, Science, and Technology, Grant-in-Aid for Scientific Research (C), 24540267, 2012, and Grant-in-Aid for Scientific Research on Priority Areas No. 467 “Probing the Dark Energy through an Extremely Wide and Deep Survey with Subaru Telescope.” This work is supported in part by JSPS (Japan Society for Promotion of Science) Core-to-Core Program “International Research Network for Dark Energy.”

[1] T. Matsubara, Phys. Rev. D, **83**, 083518 (2011).
[2] N. Bartolo, E. Komatsu, S. Matarrese and A. Riotto, Phys. Rep., **402**, 103 (2004).
[3] X. Chen, Advances in Astronomy, id.638979 (2010).
[4] J.-L. Lehnars, Advances in Astronomy, id.903907 (2010).
[5] N. Dalal, O. Doré, D. Huterer and A. Shirokov, Phys. Rev. D, **77**, 123514 (2008).

[6] S. Matarrese and L. Verde, Astrophys. J. Letters, **677**, L77 (2008).
[7] V. Desjacques, U. Seljak, Classical and Quantum Gravity, **27**, 124011 (2010).
[8] D. Wands, A. Slosar, Phys. Rev. D, **79**, 123507 (2009).
[9] A. Slosar, C. Hirata, U. Seljak, S. Ho, N. Padmanabhan, J. Cosmol. Astropart. Phys., **8**, 31 (2008).

- [10] J.-Q. Xia, M. Viel, C. Baccigalupi, G. De Zotti, S. Matarrese and L. Verde, *Astrophys. J. Letters* , **717**, L17 (2010).
- [11] J.-Q. Xia, A. Bonaldi, C. Baccigalupi, G. De Zotti, S. Matarrese, L. Verde and M. Viel, *J. Cosmol. Astropart. Phys.* , **8**, 13 (2010).
- [12] J.-Q. Xia, C. Baccigalupi, S. Matarrese, L. Verde and M. Viel, *J. Cosmol. Astropart. Phys.* , **8**, 33 (2011).
- [13] N. Afshordi and A. J. Tolley, *Phys. Rev. D* , **78**, 123507 (2008).
- [14] T. Giannantonio and C. Porciani, *Phys. Rev. D* , **81**, 063530 (2010).
- [15] F. Schmidt and M. Kamionkowski *Phys. Rev. D* , **82**, 103002 (2010).
- [16] V. Desjacques, D. Jeong and F. Schmidt, *Phys. Rev. D* , **84**, 061301 (2011).
- [17] V. Desjacques, D. Jeong and F. Schmidt, *Phys. Rev. D* , **84**, 063512 (2011).
- [18] R. Scoccimarro, L. Hui, M. Manera and K. C. Chan, *Phys. Rev. D* , **85**, 083002 (2012).
- [19] L. Verde and S. Matarrese, *Astrophys. J. Letters* , **706**, L91 (2009).
- [20] D. Jeong, E. Komatsu, *Astrophys. J.*, **703**, 1230 (2009).
- [21] P. McDonald, *Phys. Rev. D* , **78**, 123519 (2008).
- [22] A. Taruya, K. Koyama and T. Matsubara, *Phys. Rev. D* , **78**, 123534 (2008).
- [23] V. Desjacques, U. Seljak and I. T. Iliev, *Mon. Not. R. Astron. Soc.* , **396**, 85 (2009).
- [24] M. Grossi, L. Verde, C. Carbone, K. Dolag, E. Branchini, F. Iannuzzi, S. Matarrese, L. Moscardini, *Mon. Not. R. Astron. Soc.* , **398**, 321 (2009).
- [25] A. Pillepich, C. Porciani and O. Hahn, *Mon. Not. R. Astron. Soc.* , **402**, 191 (2010).
- [26] C. Wagner, L. Verde and L. Boubekeur, *J. Cosmol. Astropart. Phys.* , **10**, 22 (2010).
- [27] C. Wagner and L. Verde, *J. Cosmol. Astropart. Phys.* , **3**, 2 (2012).
- [28] K. C. Chan, R. Scoccimarro and R. K. Sheth, *Phys. Rev. D* , **85**, 083509 (2012).
- [29] F. Bernardeau, M. Crocce and R. Scoccimarro, *Phys. Rev. D* , **78**, 103521 (2008).
- [30] F. Bernardeau, M. Crocce and E. Sefusatti, *Phys. Rev. D* , **82**, 083507 (2010).
- [31] T. Buchert, *Astron. Astrophys.* , **223**, 9 (1989).
- [32] F. Moutarde, J.-M. Alimi, F. R. Bouchet, R. Pellat, and A. Ramani, *Astrophys. J.*, **382**, 377 (1991).
- [33] F. Bernardeau, *Astrophys. J.*, **472**, 51 (1994).
- [34] P. Catelan, *Mon. Not. R. Astron. Soc.* , **276**, 115 (1995).
- [35] P. Catelan and T. Theuns, *Mon. Not. R. Astron. Soc.* , **282**, 455 (1996).
- [36] T. Matsubara, *Phys. Rev. D* , **77**, 063530 (2008).
- [37] C. Rampf and T. Buchert, *J. Cosmol. Astropart. Phys.* , **6**, 21 (2012).
- [38] F. Bernardeau, S. Colombi, E. Gaztañaga, and R. Scoccimarro, *Phys. Rep.* , **367**, 1 (2002).
- [39] T. Matsubara, *Phys. Rev. D* , **78**, 083519 (2008); **78**, 109901(E) (2008).
- [40] T. Okamura, T., A. Taruya and T. Matsubara, *J. Cosmol. Astropart. Phys.* , **8**, 12 (2011).
- [41] M. Sato and T. Matsubara, *Phys. Rev. D* , **84**, 043501 (2011).
- [42] A. Gangui, F. Lucchin, S. Matarrese and S. Mollerach, *Astrophys. J.*, **430**, 447 (1994).
- [43] L. Verde, L. Wang, A. F. Heavens and M. Kamionkowski, *Mon. Not. R. Astron. Soc.* , **313**, 141 (2000).
- [44] E. Komatsu and D. N. Spergel, *Phys. Rev. D* , **63**, 063002 (2001).
- [45] P. Creminelli, A. Nicolis, L. Senatore, M. Tegmark and M. Zaldarriaga, *J. Cosmol. Astropart. Phys.* , **5**, 4 (2006).
- [46] P. D. Meerburg, J. P. van der Schaar and P. Stefano Corasaniti, *J. Cosmol. Astropart. Phys.* , **5**, 18 (2009).
- [47] L. Senatore, K. M. Smith and M. Zaldarriaga, *J. Cosmol. Astropart. Phys.* , **1**, 28 (2010).
- [48] W. H. Press and P. Schechter, *Astrophys. J.*, **187**, 425 (1974).
- [49] R. K. Sheth and G. Tormen, *Mon. Not. R. Astron. Soc.* , **308**, 119 (1999).
- [50] A. Jenkins, C. S. Frenk, S. D. M. White, J. M. Colberg, S. Cole, A. E. Evrard, H. M. P. Couchman and N. Yoshida, *Mon. Not. R. Astron. Soc.* , **321**, 372 (2001).
- [51] M. S. Warren, K. Abazajian, D. E. Holz, L. Teodoro, *Astrophys. J.*, **646**, 881 (2006).
- [52] M. Crocce, P. Fosalba, F. J. Castander and E. Gaztañaga, *Mon. Not. R. Astron. Soc.* , **403**, 1353 (2010).
- [53] H. J. Mo and S. D. M. White, *Mon. Not. R. Astron. Soc.* , **282**, 347 (1996).
- [54] H. J. Mo, Y. P. Jing, and S. D. M. White, *Mon. Not. R. Astron. Soc.* , **284**, 189 (1997).
- [55] J. R. Bond, S. Cole, G. Efstathiou, and N. Kaiser, *Astrophys. J.*, **379**, 440 (1991).
- [56] J.-O. Gong and S. Yokoyama, *Mon. Not. R. Astron. Soc.* , **417**, L79 (2011).
- [57] T. Y. Lam, V. Desjacques and R. K. Sheth *Mon. Not. R. Astron. Soc.* , **402**, 2397 (2010).
- [58] F. Schmidt, *Phys. Rev. D* , **82**, 063001 (2010).
- [59] D. Jeong, F. Schmidt, C. M. Hirata, *Phys. Rev. D* , **85**, 023504 (2012).
- [60] N. Kaiser *Mon. Not. R. Astron. Soc.* , **227**, 1 (1987).
- [61] A. J. S. Hamilton, *The Evolving Universe*, 231, 185 (1998). (astro-ph/9708102).